Pulsed Field Gradient NMR Study of Colloids

by

Swomitra Palit

A Thesis Submitted in Partial Fulfillment of the
Requirements for the Degree of

Master of Science

September 20, 2007

MEMORIAL
UNIVERSITY

Department of Physics and Physical Oceanography
Memorial University of Newfoundland
St. John's, Newfoundland
Canada

Abstract

Pulsed field gradient nuclear magnetic resonance (NMR) experiments were performed on hard-sphere-like colloidal suspensions. We synthesized NMR-visible colloidal particles and measured spectrally resolved diffusion coefficients for monodisperse suspensions of different size particles. Results of these experiments show good agreement with theoretical expectation. We also probed a bidisperse (binary) colloidal suspension successfully and obtained the diffusion coefficients of two species simultaneously. The colloidal model system developed in this work will allow the study of colloidal phase behaviour in binary mixtures for different number and size ratios.

Contents

Chapter 1

INTRODUCTION

1.1 Colloid

In 1861, Thomas Graham classified matter into two types known as crystalloids and colloids. The name colloid was derived from Greek (Kolla = glue) [1]. Diffusibility was the basis of this classification. Crystalloids (example: salt) were those substances that would diffuse through a membrane separating water from an aqueous solution and colloids (example: gelatin) were those that would not [2]. Colloids were later considered as a state of matter.

Colloidal suspensions are dispersions of particles (fluid or solid) in a fluid medium. Fog (liquid particle, gaseous medium), milk (liquid particle, liquid medium) and ink (solid particle, liquid medium) are all examples of colloids. Sizes and shapes of the colloidal particles are very important to determine the system properties. Sizes of colloids vary from 1 nm to 10 μm [3]. While there are many examples of colloidal particle that are elliptical, rodlike, disclike or random coils, the simplest colloids to study are spherical.

1.2 Interactions of Colloids

Different physical effects give rise to colloidal interactions at different length scales [4]. The interaction between colloidal particles includes long-range electrostatic interactions, short-ranged van der Waals interaction as well as hydrodynamic interactions. The simplest interaction is the excluded volume (hard-sphere) interaction. The excluded volume interaction is entropic in origin: the presence of one sphere at position (x, y, z) and at time t, affects the possible configurations at that time for all other spheres.

Figure 1.1: A shell of thickness R_G around the colloids is excluded to the centre of mass of a polymer chain. The excluded volumes add up when the colloids are far apart. But for shorter distances there are overlapping of excluded volume and hence the total volume available to the polymers increases [3].

1.2.1 Excluded Volume Interactions and the Depletion Attraction

A collection of colloidal spheres with sizes peaked sharply at one diameter is termed a monodisperse colloidal suspension. A monodisperse suspension of colloidal hard spheres interacts via the 'excluded volume interaction'- the volume of each sphere is excluded to every other sphere. The excluded volume interaction in monodisperse hard spheres leads to entropically driven colloidal phase transitions from fluid to solid phases (discussed in greater detail in Chapter 2).

A collection of large and small spheres is a bidisperse ('binary') colloidal suspension. Now if the inter-sphere distance of large spheres is less than the diameter of the small spheres, they can not penetrate in this region. There is a region of volume around each large sphere (drawn as a circle around the large spheres in Figure 1.1 and Figure 1.2) that is excluded to the center of the small spheres. If these excluded-volume regions overlap one another, the volume accessible to small spheres increases, resulting in an entropic effective attractive interaction between large spheres. This is known as the depletion attraction. In a suspension of large spheres, inclusion of small spheres (such that the ratio of the radius (size ratio) of large and small spheres > 6.7) can

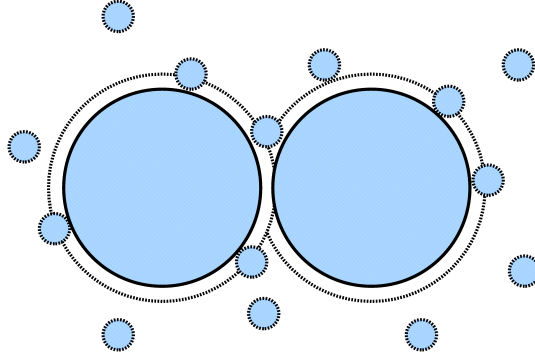Figure 1.2: Each large sphere has a zone of 'excluded volume' around it that represents the closest approach of the center of a small sphere. Overlapping of the excluded volume of large spheres (dotted contours) increases the volume accessible to the small spheres.

cause an attractive interaction between the large spheres [5]. This was first modeled by considering the presence of polymer chains in colloidal suspension.

According to Asakura and Oosawa [6], in the mixture of colloid and polymer, polymer acts like a hard sphere of radius R_G (where R_G is the radius of gyration of the polymer chain). It simply means that when the separation of colloid and polymer is less than R_G, there is an overlap between them. But as shown in Figure 1.1, if the polymer-colloid are far apart, the polymer can have less conformations than when the colloidal particles are close together. Here two colloids of radius R are at a distance which is more than $2(R + R_G)$. So colloids excluded a volume $\frac{4}{3}\pi(R + R_G)^3$ to the centre of mass of the polymer chains. The 'depletion' region of thickness R_G, where there is no colloid and a lower than average concentration of polymer, creates an osmotic pressure (pressure caused by the different concentration of solute usually in a system containing a semi-permeable membrane) due to the concentration gradient of polymer chains inside and outside of the sphere.

Figure 1.2 shows a binary mixture where the volume around the spheres that is the excluded volume for the small spheres overlaps, thus reducing the total excluded volume, and introducing an effective (depletion) attraction. Increasing small sphere concentration increases the strength of attraction. It also depends on the radius of the small spheres. This interaction is strong

Figure 1.3: Schematic diagram of ions and counterions from spherical particles. Small filled circles indicate the atoms of the colloids.

enough for entropy driven phase transitions.

1.2.2 Electrostatic Interactions

According to Coulomb's law, in vacuum, the electrostatic interaction energy between two charged particles (or ions) at center to center distance r

$$U(r) = \frac{q_1 q_2}{4\pi\epsilon_0 r} \tag{1.1}$$

where $\epsilon_0 = 8.85 \times 10^{-12}$ N m^2 / C^2.

The interaction energy is long-ranged because it is proportional to the inverse of the distance r.

But instead of a vacuum, if the charged particles (or ions) are interacting in a dielectric medium then Equation 1.1 can be written as

$$U(r) = \frac{q_1 q_2}{4\pi\epsilon r} \tag{1.2}$$

where $\epsilon = \epsilon_r \epsilon_0$ and ϵ_r is known as the dielectric constant of the medium. In the case of water at 20^0C, $\epsilon_r \approx 80$. The effect of the dielectric medium reduces the interaction energy. This is known as dielectric screening of the charge. In the presence of free ions, the interaction reduces further.

The electrostatic interaction between a charged surface and free charges in solution plays an important role in colloidal systems. Because of the ions on the surface, a cluster of opposite charged ions in solution (called 'counterions') gather around it and form a diffuse layer as shown in Figure 1.3

6

[7]. The surface ions and the cloud of counterions form the electrical double layer. The thickness of the double layer is κ^{-1}, known as the Debye-Hückel screening length. Charged colloidal spheres interact with the counterions of the solvent by a screened Coulomb interaction that has the form [8]

$$U(r) \approx \lambda \frac{exp(-\kappa r)}{r} \tag{1.3}$$

The potential decreases exponentially with distance around a spherical particle. The Debye-Hückel screening length can be controlled experimentally by controlling solvent parameters:

$$\frac{1}{\kappa} = \frac{1}{e}\sqrt{\frac{\epsilon K_B T}{2 c N_a}} \tag{1.4}$$

where e is the electronic charge, c is the molar concentration of salt, N_a is the Avogadro's number, T is the temperature and K_B is the Boltzmann constant. The Debye-Hückel screening length, κ^{-1}, is a key parameter that measures the contribution of valency, concentration and dielectric constant to the screening of interactions between charges in solutions.

Now if two charged colloids of radius a approach to each other, there is a repulsive force that push them apart. In this case the effect of the diffuse layer plays a dominant role. According to Derjaguin-Landau-Verwey-Overbeek, the repulsive interaction potential (known as DLVO potential) in SI units is [9]:

$$U_R(r) = 2\pi\epsilon a\psi_0^2 \ln[1 + \exp\{-\kappa(r - 2a)\}] \tag{1.5}$$

where $\psi_0 = \dfrac{\sigma}{\epsilon\kappa}$, the particle surface potential and σ is the surface charge per unit area. From Equation 1.5, for $r > 2a$, when the Debye screening length κ^{-1} is short, i.e when $\kappa(r - 2a)$ is large, the repulsive potential goes to zero.

1.2.3 Van der Waals Interaction

In molecules and atoms, electrons move around the nucleus and create an instantaneous dipole. The rapidly changing dipole produces an induced dipole moment to neighbouring atoms. In the vacuum, the induced dipole of the neighbouring atom moves in phase with the original dipole and hence there exists an attractive atomic interaction [10]. The interaction of two atoms i and j separated by a distance r_{ij} is [7]

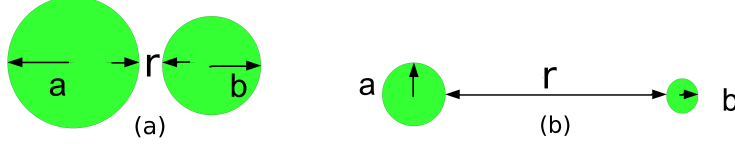$$U(r) \equiv \frac{-C_{ij}}{r_{ij}^6} \tag{1.6}$$

Figure 1.4: Different distance regimes for the van der Waals interaction between two spheres of radius a and b (a) $a, b \gg r$ and (b) $a, b \ll r$.

Here C_{ij} is the London's constant and its value depends on the atomic numbers of two interacting atoms. $U(r)$ is known as the London dispersion interaction.

The London dispersion interaction can be extended to the interaction between two colloidal spheres. For this calculation all the pairwise interactions between the atoms (Figure 1.3) of each colloidal particle have to be added up.

For $a, b \gg r$ (shown in Figure 1.4(a)), the van der Waals interaction can be written as [11]

$$U(r) = \frac{-A}{6r}\left(\frac{ab}{a+b}\right) \tag{1.7}$$

and when $a, b \ll r$, (shown in Figure 1.4(b))

$$U(r) = \frac{-16A}{9}\left(\frac{a^3 b^3}{r^6}\right) \tag{1.8}$$

So the van der Waals interaction between two colloidal particles of the same material immersed in a fluid is always attractive. Equation 1.7 and Equation 1.8 suggest that the potential becomes infinitely negative on contact so that particles once in contact could never be redispersed. But practically redispersion is often possible due to other forces at very small separation. Here A is known as the Hamaker constant and it depends on material properties (see Table 1.1). So it changes with the combination of materials.

In the case of two polystyrene particles separated by one-tenth of particle diameter (0.99 μm) in water, the attractive potential is $\approx$ -10^{-17} J. But when the particles are two particle diameters apart, the potential becomes $\approx$ -10^{-23} J. So, when particles are approximately more than one particle diameter apart, the van der Waals attraction is less than $K_B T$ (4×10^{-21} J), K_B is Boltzmann's constant and T absolute temperature. In actual fact, the polystyrene spheres used in this study are surrounded by a surfactant

Table 1.1: Hamaker Constants $(\times 10^{21})$/J for two combinations of materials M [8].

Material	M-Air-M	M-Water-M
Water	3.7	0
Alkanes		
n=5	3.8	0.3
n=6	4.1	0.4
n=10	4.8	0.5
n=14	5.1	0.5
n=16	5.2	0.5
Fused quartz	6.5	0.8
Fused Silica	6.6	0.8
Sapphire	16	5
Polymethyl methacrylate	7.1	1.1
Polystyrene	6.6	1.0
Polyisoprene	0.6	0.7
Mica (green)	10	2.1

stabilizer, which both reduces the effective Hamaker constant, and increases the distance of closest approach between two spheres.

1.2.4 Hydrodynamic Interaction

In a colloidal suspension, the movement of particles cause dynamical effects. When a colloidal particle of radius a moves, it creates a flow in the incompressible liquid. Other particles in the suspension are influenced by the flow [12]. As an effect of flowing intervening liquid, all the particles in the suspension see each other. This effect is known as the hydrodynamic interaction. There is no analogy of hydrodynamic interaction in atomic and molecular systems. The velocity of the flowing liquid obeys the Navier-Stokes equation for an incompressible fluid [3] which is

$$\rho\frac{\partial \vec{v}(r,t)}{\partial t} + \rho\vec{v}(r,t)\cdot\nabla\vec{v}(r,t) = -\nabla p(r,t) + \eta\nabla^2\vec{v}(r,t) \qquad (1.9)$$

where $\vec{v}(r,t)$ is the flow velocity at point r and time t, ρ is the density of the solvent and $p(r,t)$ is the hydrostatic pressure. In dimensionless notation, the Navier-Stokes equation has the form [13]

$$\frac{\partial \vec{v}\,'(r,t)}{\partial t'} + \vec{v}\,'(r,t)\cdot\nabla'\vec{v}\,'(r,t) = -(\frac{1}{\rho U^2})(\frac{\eta U}{L})\nabla'p\,'(r,t) + \frac{\eta}{UL\rho}\nabla'^2\vec{v}\,'(r,t) \qquad (1.10)$$

Here $\vec{v}\,' = \dfrac{\vec{v}}{U}$, $t\,' = \dfrac{tU}{L}$, $p\,' = \dfrac{pL}{\eta U}$ where L, U are typical length scales and velocity scales and $\dfrac{L}{U}$ is therefore a typical timescale in the system.

$$\text{Also } \nabla' = L\nabla \text{ and } \frac{\partial}{\partial t'} = \frac{L}{U}\frac{\partial}{\partial t}$$

From L, U and the density ρ, one can construct a dimensionless number $Re = \dfrac{UL\rho}{\eta}$, known as the Reynolds number.
Now from the Equation 1.10 [2]

$$Re\left[\frac{\partial \vec{v}\,'(r,t)}{\partial t'} + \vec{v}\,'(r,t)\cdot\nabla'\vec{v}\,'(r,t)\right] = -\nabla'p\,'(r,t) + \nabla'^2\vec{v}\,'(r,t) \qquad (1.11)$$

Reynolds number is the ratio of inertial force to viscous force. When $Re << 1$, the viscous force dominates over inertial force. But for $Re >> 1$, inertial force dominates. For example, for a polystyrene sphere (radius, $a = 0.5\mu$m) moving at 1 μm/s in water (viscosity, $\eta = 8.90\times10^{-4}Pa.s$) has the Reynolds

number $\approx 10^{-6}$. Thus in the case of colloidal particles moving in liquid, the inertia is very small. So the inertia term, $\vec{v}(r,t) \cdot \nabla \vec{v}(r,t)$, can be neglected and Equation 1.10 becomes

$$\rho \frac{\partial \vec{v}(r,t)}{\partial t} = -\nabla p(r,t) + \eta \nabla^2 \vec{v}(r,t) \qquad (1.12)$$

This is the Stokes equation for a viscous fluid. In the case where the flow is steady $(\frac{\partial \vec{v}(r,t)}{\partial t}) = 0$

$$\eta \nabla^2 \vec{v}(r,t) = \nabla p(r,t) \qquad (1.13)$$

This is known as the creeping-flow equation [14]. Flow around colloidal particles can be described by using this equation. Thus, in a quiescent suspension, when a sphere moves under the influence of gravity, the hydrodynamic force acting on it can be expressed as [14]:

$$\vec{F} = -6\pi \eta a \vec{v}(r,t) \qquad (1.14)$$

Hence $\mu = 6\pi \eta a$ is known as friction coefficient. The Stokes-Einstein relation relates the particle diffusion coefficient to the friction coefficient [8]:

$$D = \frac{K_B T}{\mu} \qquad (1.15)$$

where K_B is Boltzmann's constant and T absolute temperature. The friction coefficient increases with the increasing number of particles and as a result the diffusion gets slower. The diffusion coefficient measured in a colloidal suspension is thus dependent on the particle density. One characteristic of colloidal systems approaching glass transition is the breakdown of the Stokes-Einstein relation. In our studies the Stokes-Einstein relation in dilute suspensions will be an important test of the validity of our experimental methods.

1.3   Sedimentation

Sedimentation is the settling of colloidal particles under the influence of gravity. The settling velocity of a polystyrene sphere of radius a is [7]

$$V_0 = \frac{2a^2 \Delta \rho g}{9\eta} \qquad (1.16)$$

$\Delta \rho$ is the density difference between the sphere and surrounding liquid. This equation is valid only for a highly dilute system. In the case of a two particle

11

system having a difference in settling velocity equal to ΔV_0, the flow velocity of each particle affects the other one. This perturbation is described by the Peclet number for sedimentation [2], which is given by:

$$Pe = \frac{2a\Delta V_0}{D_0} \qquad (1.17)$$

D_0 is the diffusion coefficient at infinite dilution. For a polystyrene sphere of 1 μm diameter in water, $Pe = 0.05$. For $Pe \ll 1$, the particles are exhibiting Brownian motion while for $Pe \gg 1$, hydrodynamic interaction is dominant over Brownian motion. But in the regime of concentrated suspension, the settling velocity of each particle is affected by the others in a complicated way. The concentration dependence of the sedimentation velocity is [15]

$$V(\phi) = V_0(1 + A\phi) \qquad (1.18)$$

In the presence of hydrodynamic interaction, for the zeroth order correction, $A = -6.55$ [16]. The magnitude and sign of A are due to the large contribution from backflow.

1.4   Model Hard-Sphere Colloids

Colloids have been used as a model for atomic and molecular systems as they demonstrate many of the phases observed in such systems. The simplest model is the hard sphere system in which the colloids are non interacting at all separations beyond their radius and infinitely repulsive on contact [17]. In this case, the long-range electrostatic interaction effect becomes negligible. Experimentally this is done by decreasing the Debye-Hückel screening length of Equation 1.4. As was discussed in this chapter, van der Waals interaction are not weak for polystyrene spheres when interparticle separation is less than one-tenth of particle diameter in an aqueous suspension.

We mentioned that in a true model hard-sphere system there is only excluded volume interaction. Our system is not an 'ideal' hard sphere system. It is 'hard-sphere-like' because the dominant electrostatic repulsive interactions are screened sufficiently. Van der Waals attractions are probably present, but are reduced by the presence of surfactant stabilizer. Finally, except in the dilute limit, hydrodynamic interactions are always important in colloidal dynamics.

Chapter 2

COLLOIDAL DISPERSIONS

The word 'colloidal dispersion' refers to colloids of different sizes and states (eg. solid, liquid or gas) dispersed in a continuous phase of a different state [18]. Depending on the size distribution of particles, the dispersion will be either monodisperse (a size distribution that has a single narrow peak) or polydisperse (multiple peaks in the size distribution).

2.1 Monodisperse Hard Spheres: Phase Behavior & Dynamics

2.1.1 Phase Transition of Monodisperse Hard Spheres

From a thermodynamic point of view, for microscopic systems one can write a free energy (F) in terms of an internal energy (U) and an entropy (S)

$$F = U - TS \tag{2.1}$$

Thus increasing temperature increases the stability of phases that are more disordered (have higher entropy). For a hard sphere system, the analogue of internal energy is the interaction between spheres (which is zero, with the constraint that spheres do not overlap). In atomic systems, the internal energy is temperature-dependent and is lower for more ordered phases, while the entropic term ($-TS$) is lower at high temperatures. Thus there is a temperature-driven competition between order and disorder. In hard-sphere colloids, the internal energy contribution is temperature independent, so phase changes are driven by change in entropic term with increasing volume fraction, ϕ. So, here, instead of temperature, the relevant thermodynamic variable is the particle volume fraction (ϕ) that determines the phase
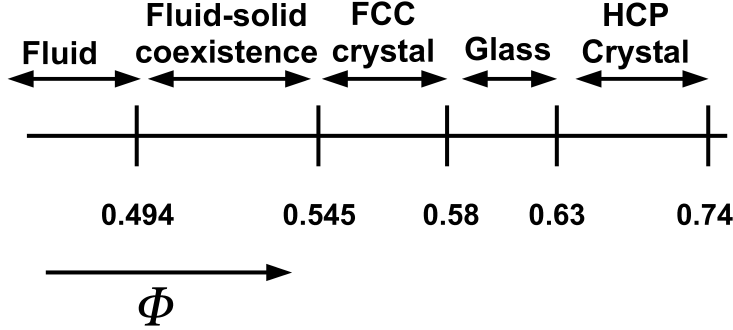
Figure 2.1: Phase diagram as a function of volume fraction (ϕ) of a model hard sphere system [19]. Here FCC and HCP refers to 'face centered cubic' and 'hexagonal closed packed' respectively.

behaviour of hard-sphere colloids. The volume fraction ϕ is related to number density n by:

$$\phi = (4\pi/3)a^3 n \ , \ a \text{ is the particle radius.}$$

In a dilute system ($\phi \to 0$) the mean sphere separation is large. As the volume fraction increases, there are spatial correlations between the positions of the spheres.

Colloidal systems show a rich phase diagram from fluid to crystal including a glass phase (Figure 2.1). At low packing fraction, the fluid phase is stable because it has higher entropy. But above ($\phi = 0.545$), the ordered solid phase is actually entropically favored. This is because disorder would confine several particles in volumes significantly smaller than the crystal cage volume. So the crystal phase is stable [20]. This phase persists from ($\phi = 0.545$) to 0.740, the maximal packing of monodisperse spheres. But at $\phi = 0.58$, the crystallization of the colloids can be (under some circumstances e.g particle polydispersity) arrested [21] by the appearance of a metastable state known as a glass which is characterized by a large increase in the viscosity of the system [22]. The hard-sphere phase diagram is purely entropic in nature.

2.1.2 Dynamics of Monodisperse Hard Spheres

Colloidal particles are in constant motion due to Brownian motion, caused by the molecular nature of the surrounding fluid medium. According to

the Stokes-Einstein relation, the diffusion coefficient of spherical particles of hydrodynamic radius a suspended in a solvent of viscosity η is described by:

$$D_0 = \frac{K_B T}{6\pi\eta a} \tag{2.2}$$

where K_B is Boltzmann's constant and T absolute temperature. This relation is only valid for dilute dispersions, where the interaction between Brownian particles can be neglected. According to this relation at room temperature, the diffusion coefficient of a 1 μm particle suspended in water is $\approx 5 \times 10^{-13}$ m^2/s.

For interacting particles things are more complicated. In that case the translational self-diffusion of a labeled colloidal particle in an environment of other colloidal particles can be divided into three different regimes depending on the timescale [14]. For $t < \tau_B$ particles' motion is ballistic (not random). The Brownian time, τ_B, equals to $m/6\pi\eta a$. Another characteristic time τ_1 is ξ^2/D_0, ξ is the interparticle interaction distance. The second regime describes the motion of the colloidal particles over distances much shorter than the interparticle distance. So, in the time scale $\tau_B << t << \tau_1$, the mean-square displacement $\langle |r(t) - r(0)|^2 \rangle$ is only influenced by the hydrodynamic interaction, where $r(t)$ denotes the instantaneous displacement at time t. Hence the diffusion of individual particles can be defined by a short time self-diffusion coefficient D_s^S

$$\langle |r(t) - r(0)|^2 \rangle = 6D_s^S t \text{ , when } \tau_B << t << \tau_1$$

For a particle of diameter equals to 1 μm in water, $\tau_B = 6.5 \times 10^{-5}$ ms and $\tau_1 \approx 500$ ms.

The third regime describes the self diffusion at times larger than τ_1 where direct interactions between particles play an important role and hence the mean square displacement can be defined by a long time self-diffusion coefficient D_s^L

$$\langle |r(t) - r(0)|^2 \rangle = 6D_s^L t \text{ , when } t \gg \tau_1$$

Due to self-diffusion, a local fluctuation in concentration can occur in the dispersion when particles at higher concentration diffuse towards the lower concentration region. This diffusion process is known as mutual diffusion.

The dependence of self-diffusion coefficients on the particle volume fraction ϕ for hard spheres in an equilibrium configuration of other particles can be

15

Table 2.1: Values of hydrodynamic coefficients for the volume fraction dependence of the short-time and long-time diffusion coefficients obtained by different studies [14] .

K_s^S	K_s^L	Reference
-1.83	-2.68	Batchelor [23] (theory)
-1.73	-	Felderhof [24], Muthukumar and Freed [25] (theory)
-	-1.89	Felderhof [26] (theory)
-2	-	Yoshida [27] (theory)
-	-2.1	Cichocki and Felderhof [28] (theory)
-	-2.91 ± 0.03 & -2.83 ± 0.07	Blees, Geurts, Leyte [29] (experiment)
-1.6	-	Wassenius, Nydén, Vincent [30] (experiment)

described by

$$D_s^S = D_0(1 + K_s^S\phi) \tag{2.3}$$

and

$$D_s^L = D_0(1 + K_s^L\phi) \tag{2.4}$$

which is first order in ϕ and is valid for dilute suspensions. Different authors reported different values of the coefficients K_s^S and K_s^L (see Table 2.1).

But according to a mean-field approximation of Mazur and Geigenmüller [31]

$$D_s^S = D_0\frac{1 - \phi}{1 + (3/2)\phi} \tag{2.5}$$

Also a theoretical work of Medina-Noyola [32] and the calculation of van Blaaderen [33] that uses Equation 2.5 gives

$$D_s^L = D_0\frac{(1 - \phi)^3}{[1 + (3/2)\phi + 2\phi^2 + 3\phi^3]} \tag{2.6}$$

Note that even in the short time limit, the short-time diffusion coefficient is not identical to D_0 because of hydrodynamic interactions. At long times the diffusion of particles is affected by the proximity of a cage of surrounding particles as well as hydrodynamic interactions.

16

2.2 Polydisperse Hard Spheres: Phase Behavior & Dynamics

2.2.1 Phase Transition of Polydisperse Hard Spheres

The entropic contribution to the colloid free energy can be controlled by introducing polydispersity. It is found that inclusion of small spheres can increase the entropy of the system of ordered large spheres [6]. Also it can result in an attractive depletion force between large spheres for the size ratio greater than 6.7 [5]. Polydispersity has a significant influence on crystallization [34].

The simplest form of polydispersity is bidispersity. A mixture of large and small particles (labeled as i and j in what follows) is commonly referred to as a binary mixture. Where volume fraction ϕ is the only parameter involved with single particle dynamics, a binary mixture requires, in addition, the ratio of the radius a_j/a_i and the relative volume fraction ϕ_j/ϕ of the smaller particles. One can also alter the phase diagram by varying the particle shape (non-spherical objects pack differently from spherical objects) or by introducing polydispersity in particle size. In general, polydispersity inhibits crystallization. Therefore a control of polydispersity allows researchers to study the colloidal glass transition. Experimentally it was found that particles with a size distribution skewed to smaller sizes crystallized an order of magnitude more slowly than particles with a more symmetrical distribution [35, 36]. So polydispersity introduces new control parameters, particle size ratios and particle number ratios, to make quantitative tests to compare with theory and simulation.

2.2.2 Dynamics of Polydisperse Hard Spheres

The short time self diffusion coefficient of a tracer particle k which is at vanishingly low volume fraction of a general binary mixture of i and j can be written as [15].

$$\frac{D_s^S(k)}{D_0(k)} = 1 + K_{ki}\phi_i + K_{kj}\phi_j \tag{2.7}$$

Results for the diffusion coefficients of i and j can be extracted from the above equation by considering the tracer particle k that is identical to either species i or j. If k is identical with i, then

Table 2.2: K_{ij} as a function of size ratio

Size ratio (a_j/a_i)	K_{ij}
0	-2.50
0.125	-2.31
0.25	-2.17
0.5	-1.94
1	-1.56
2	-1.10
4	-0.63
8	-0.24

$$\frac{D_s^S(i)}{D_0(i)} = 1 + K_{ii}\phi_i + K_{ij}\phi_j \tag{2.8}$$

And for k identical with j

$$\frac{D_s^S(j)}{D_0(j)} = 1 + K_{jj}\phi_j + K_{ji}\phi_i \tag{2.9}$$

This is valid for dilute suspensions. Explicit results for K_{ij} as a function of size ratio were calculated by Batchelor (Table 2.2) [37].

The coefficients K_{ij} depend solely on size ratio, a_j/a_i, and are always negative. It describes the slowness in diffusion for the interaction of i particles with j type particles. It was found that the calculated values of K_{ij} in Table 2.2 are fitted well by the simple empirical relation [38]

$$K_{ij} = -\frac{2.5}{1 + 0.6(a_j/a_i)} \tag{2.10}$$

Following Equation 2.10, for the binary mixture of 0.99 μm and 0.79 μm particles, K_{ij}= -1.43 and K_{ji}= -1.69, whereas $K_{ii} = K_{jj}$ = -1.56.

2.2.3 The Glass Transition and Binary Colloidal Mixtures

The entropic effect of a two-component system consisting of small and large spheres can be interpreted as the small spheres modifying the effective interaction of the large spheres. The fluid-glass transition of soft spheres has been

investigated by extensive molecular dynamics simulation for the size ratio of 1.2 [39]. Other molecular dynamics simulations of the size ratios of 0.60 and 0.83 were done to study the binary hard sphere liquids [40]. Mode-coupling theory is also used extensively to study the glass transition [41].

Experimental study of the glass transition includes dynamic light scattering (DLS), fluorescence recovery after photobleaching (FRAP) and confocal microscopy. Investigation of DLS suggests that the metastable fluid or glass states in binary mixtures persist long enough (because of exceedingly slow crystallization compared to monodisperse suspensions) to study their dynamical properties [42]. A FRAP study found two different glassy states at high volume fractions [43]. Confocal microscopy confirms the increase in cluster size near the glass transition [44]. A study of a binary system was performed using FRAP with the ratio of radius 1:9.3 [45]. Another study of a binary colloidal suspension of PMMA spheres (size ratio 0.61 and number ratio $\geq$ 0.66 of large spheres) was done via light scattering [46] and found coexistence of crystalline and fluid phase.

Experimental studies of phase behavior and dynamics as a function of particle size ratios and number ratios would allow detailed comparisons with theory.

2.3 Previous Experimental Studies of Colloidal Dynamics

Among the techniques used to study colloidal systems, the scattering of radiation has proved to be one of the most useful since it allows measurements to be made of both the spatial and the temporal correlation between the particles [47, 48]. Light and neutron beams appear to have been the forms of radiation most widely used for these studies [49]. Dynamic light scattering (DLS) experiments is a powerful tool to study the static and dynamical properties of colloidal suspensions. The following description of DLS technique follows the discussion in Wagner, Härtl and Walderhaug [50] closely. DLS experiments on monodisperse and optically isotropic particles determine the intermediate scattering function $S(Q,t)$.

$$S(Q,t) = \frac{1}{N}\langle\sum_{i}^{N}\sum_{j}^{N} exp(iQ(R_i(0) - R_j(t)))\rangle \qquad (2.11)$$

which is the spatial Fourier-transform of the pair-correlation function. (The pair-correlation function is related to the probability of finding the center of

a particle a given distance from the center of another particle [51] and is a quantity calculable directly via computer simulations). Here, Q denotes the scattering wave vector and R_i the center of mass vector of the ith particle. The double sum can be divided into two parts

$$S(Q,t) = \frac{1}{N}[\langle\sum_i^N exp(iQ(R_i(t)-R_i(0)))\rangle + \langle\sum_i^N\sum_{j\neq i} exp(iQ(R_i(t) - R_j(0)))\rangle]$$

And hence

$$S(Q,t) = S_s(Q,t) + S_d(Q,t) \qquad (2.12)$$

where $S_s(Q,t)$ is the self part and $S_d(Q,t)$ is the distinct part of the intermediate scattering function. Here self part describes the intensity correlation of same particle at two different times ($t = 0$ to t). On the other hand, the distinct part originates from the correlation of a particle i at a time $t = 0$ with a different particle j at a time t. In a system of N-particles, there are N contributions from the self part but $N(N-1)$ contributions to the distinct part of the intermediate scattering function. Therefore, light scattering experiments performed using suspensions consisting of identical particles are dominated by collective phenomena. Nevertheless, self parts are accessible by tracer experiments by means of light scattering [52]. To avoid the unwanted scattering of light particles must be matched in refractive index with the solvent.

Laser scanned confocal microscopy is also a powerful technique to study the dynamics of colloidal suspensions [53] . The fundamental requirement is that the index of refraction of the fluorescent labeled colloidal spheres must be closely matched with that of the solvent. Otherwise heavy scattering of light places restrictions on our ability to look deep inside the sample. In confocal microscopy, laser light excites fluorescence in the fluorescent-dyed particles (without the fluorescent dye excitation, the particle in a refractive-index matched solvent would be invisible). The laser scans the sample along the plane and from the emitted light a two-dimensional image can be obtained. The information about third dimension is achieved simply by looking at different depths of the sample. Development of image processing techniques allows one to track the motion of individual colloidal particles which in turn provides information about the dynamics of the system [54].

Fluorescence Recovery After Photobleaching (FRAP) is another technique which measures self-diffusion of fluorescent-labeled colloidal particles [55]. In the first step of FRAP, a well-defined part of the sample is illuminated

20

by an intense light pulse. This irreversibly photobleaches the fluorophores in the region illuminated within the sample. After the short pulse the intensity of the incident radiation is greatly reduced. The fluorescent intensity is then monitored as a function of time. The bleach pattern gradually fades away as a result of the Brownian motion of the labeled species. The exchange of bleached and unbleached particles gives rise to a change in measured fluorescent intensity. The rate at which this process takes place is related to species' diffusion coefficient.

Pulsed-Field Gradient (PFG) NMR is a prominent tool to measure self-diffusion in complex fluids [56]. It is now a common method for the study of diffusion in liquid surfactant and polymer systems [57]. For heterogeneous systems such as macroscopic emulsions, the droplet size distribution can be investigated by the PFG-NMR technique [11]. Due to the very rapid relaxation of solid materials, colloidal systems where the dispersed phase is in a solid state are difficult to study with the PFG-NMR technique. Because of high gyromagnetic ratio, the nucleus which is most suitable for PFG-NMR measurements is ^{1}H. The polymer chains of latex colloidal particles have a high content of ^{1}H ideally suited for PFG-NMR experiments. However, it turns out that in most widely used latex spheres systems, such as polystyrene and polymethylmethacrylate, the local reorientational mobility of polymer segments is very low. This low mobility causes a very fast decay of the NMR signal due to relaxation, which makes ^{1}H PFG-NMR measurements on these systems difficult. There are two reports of NMR studies of colloid diffusion where polybutadiene or polybutylacrylate spheres with high molecular reorientational mobility (as compared with other polymers) have been used for diffusion measurements [50, 29]. But the problem with the use of even such polymer spheres is that only a small fraction of the polymer chains have enough mobility to give rise to an NMR signal. So if a larger part of the particle volume contributed to the NMR signal, the PFG measurements of colloidal diffusion could be significantly improved. For this purpose, latex particles (polystyrene) with a liquid core were studied for measuring the translational particle dynamics [30]. PFG NMR results in suspensions of these core-shell spheres were analyzed by taking into account diffusion of the oil inside the spheres as well as the overall diffusion of the sphere itself. A primary short-coming of this system, however, was the large and uncontrolled polydispersity in size, which prevented the study of colloidal phase behavior. Moreover no study has been done so far on binary colloidal suspensions using NMR.

2.4 A Model System for NMR Studies of Binary Colloids

The primary advantage of using NMR are that it can be used on transparent or opaque suspensions, and even in highly concentrated suspensions. Reported in this thesis is a proof of principle for studying bidisperse colloids in a model-independent way, something that is exceedingly challenging via scattering techniques. While bidisperse colloids in transparent suspensions can indeed be studied by confocal microscopy, this one is limited by practical consideration to size ratios of $\approx$ 3:1 or less. The FRAP technique can also be used to study bidisperse colloids, but reports only on the long-time self diffusion coefficient. The NMR technique reported can provide information on short- and long-time self diffusion coefficients in opaque, concentrated colloidal suspensions.

In a study of binary colloids using DLS, the scattered light intensity has information from both the particle species simultaneously. Also both the particles and solvent have to be refractive index matched. Using the confocal microscope, study of the small particles (diameter < 0.5 μm) is not possible because of its limitation in spatial resolution. In this thesis we present PFG-NMR measurements on polystyrene particles in water. The study includes the dynamics of mono-disperse colloidal suspensions as well as that of binary (bi-disperse) suspensions where two particle species have different size. The goal is to study both species simultaneously. This requires two species to have distinct NMR signals. We have devised a new model system where one can measure the diffusion coefficients of all components of an opaque, multi-component colloidal suspension for any size ratios.

Chapter 3

PULSED FIELD GRADIENT NMR SPECTROSCOPY

Pulsed-field gradient NMR spectroscopy is an important tool for measurement of molecular translational motion. In the presence of a field gradient, the translational diffusion of molecules reduces the intensity of the NMR spin echo signal. Careful measurement of this signal attenuation provides useful information about the diffusion process. Pulsed-field gradient (PFG) NMR is a powerful measurement technique that can provide a quantitative measure of molecular motion over the millisecond to second time scale [58].

3.1 Introduction to Nuclear Magnetic Resonance

Nuclear Magnetic Resonance is a quantum mechanical phenomenon which is based on the magnetic properties of the nucleus. It occurs when the nuclei of certain atoms are immersed in a static magnetic field and exposed to a second oscillating magnetic field. In a nucleus, the proton possesses a property called spin which can be thought of as a small magnetic field and will cause the nucleus to produce an NMR signal.

The NMR spectrometer is basically an instrument capable of generating a nuclear magnetization with a large applied magnetic field, rotating the spin polarization via radiofrequency pulses to produce a transverse magnetization, and detecting tiny electric currents induced by the precession of this transverse magnetization [59].

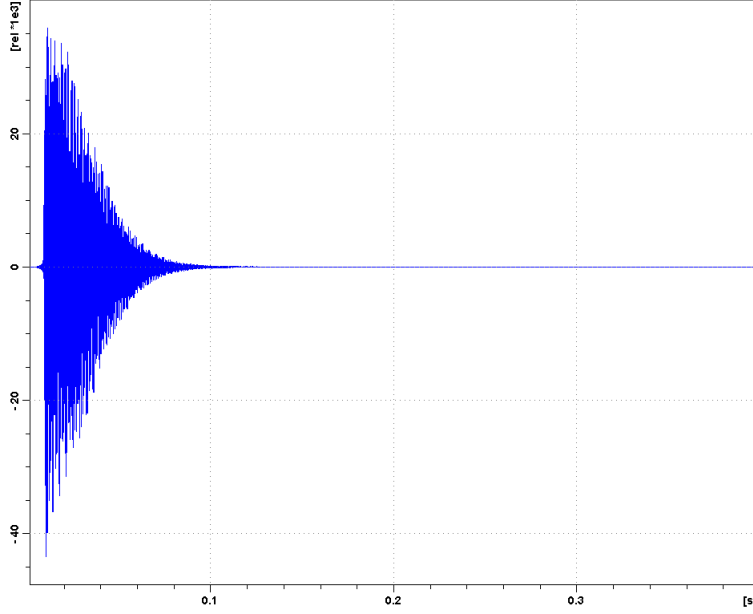In a system of randomly oriented nuclear spins, the effect of an external

Figure 3.1: Free induction decay for a one dimensional single pulse experiment.

magnetic field B_0 (along Z direction) gives rise to precession along the direction of the field. The precession frequency ω_0 , known as Larmor frequency, can be expressed as

$$\omega_0 = \gamma B_0 \tag{3.1}$$

where γ is the gyromagnetic ratio which is an intrinsic property of any nucleus ($\gamma_{1_H} = 26.752 \times 10^7$ s^{-1} T^{-1} and $\gamma_{2_H} = 4.107 \times 10^7$ s^{-1} T^{-1}).

The simplest possible NMR experiment is referred to here as a one-dimensional single pulse experiment or '90^0-FID' experiment, where the magnitude of the radiofrequency (rf) pulse is chosen carefully such that the resultant magnetization is exactly along the Y-axis (this is called a 90^0 pulse). Usually (in high-resolution NMR experiments) this is done by keeping the rf pulse amplitude fixed but varying the pulse duration. There is a mathematical trick to deal with spin dynamics in the presence of an rf field. Viewing the spins from a reference frame rotating (about the Z axis) with the resonant part of the rf field, it is possible to make the rf field look static [59]. In the rotating frame, one may think of an 90^0 rf pulse along the X axis. The net magnetization vector is then rotated down into the XY plane and begins to precess about the Z axis. The small oscillatory electric currents induced by

the precession of transverse magnetization is observed as the free-induction decay (FID)(Figure 3.1).

3.2 Relaxation in NMR

Generally the term 'relaxation' is used for the re-establishment of thermal equilibrium of a perturbed system (a system that obeys the Boltzmann distribution function). In the presence of a magnetic field, if a sample is undisturbed for a long time, it reaches a state of thermal equilibrium. But a radio frequency pulse perturbs the system to a non-equilibrium state. Relaxation is the process of regaining the equilibrium of a spin system through interactions with environment. Relaxation processes in NMR are roughly divided into two types: spin-lattice relaxation and spin-spin interaction.

3.2.1 Spin-lattice Relaxation

As shown in Figure 3.2(a), in the presence of a static magnetic field B_0, the net magnetization vector is parallel to the direction of B_0 and $M_Z = M_0$. This equilibrium system is perturbed by an oscillating radio-frequency magnetic field (B_1) which is perpendicular to B_0. When a 90^0 rf X-pulse is applied, the magnetization is flipped (in the rotating reference frame) from the Z-axis to the Y axis (Figure 3.2(b)) and hence $M_Z = 0$ and $M_Y = M_0$. But switching the radio frequency pulse off causes the magnetization to relax back to its equilibrium value ($M_Z = M_0$, $M_Y = M_X = 0$). This relaxation is well known as spin-lattice relaxation or T_1 relaxation. The relaxation time depends on factors such as the type of nucleus, sample, temperature and the viscosity. Experimentally T_1 can be measured by a technique known as inversion recovery (Figure 3.3). In this sequence, a 180^0 pulse (a pulse of same amplitude as the 90^0 pulse, but twice as long) is first applied. This rotates the net magnetization down to the $-Z$ axis. The magnetization undergoes spin-lattice relaxation and returns toward its equilibrium position along the $+Z$ axis. Before it reaches equilibrium, a 90^0 pulse is applied which rotates the longitudinal magnetization into the XY plane, and the FID is measured. This pulse sequence is repeated for several values of τ and the signal can be written as

$$S \propto (1 - 2\exp(-\tau/T_1)) \tag{3.2}$$

It should be noted at this time that the zero crossing of this function occurs for $\tau = T_1 \ln 2$.
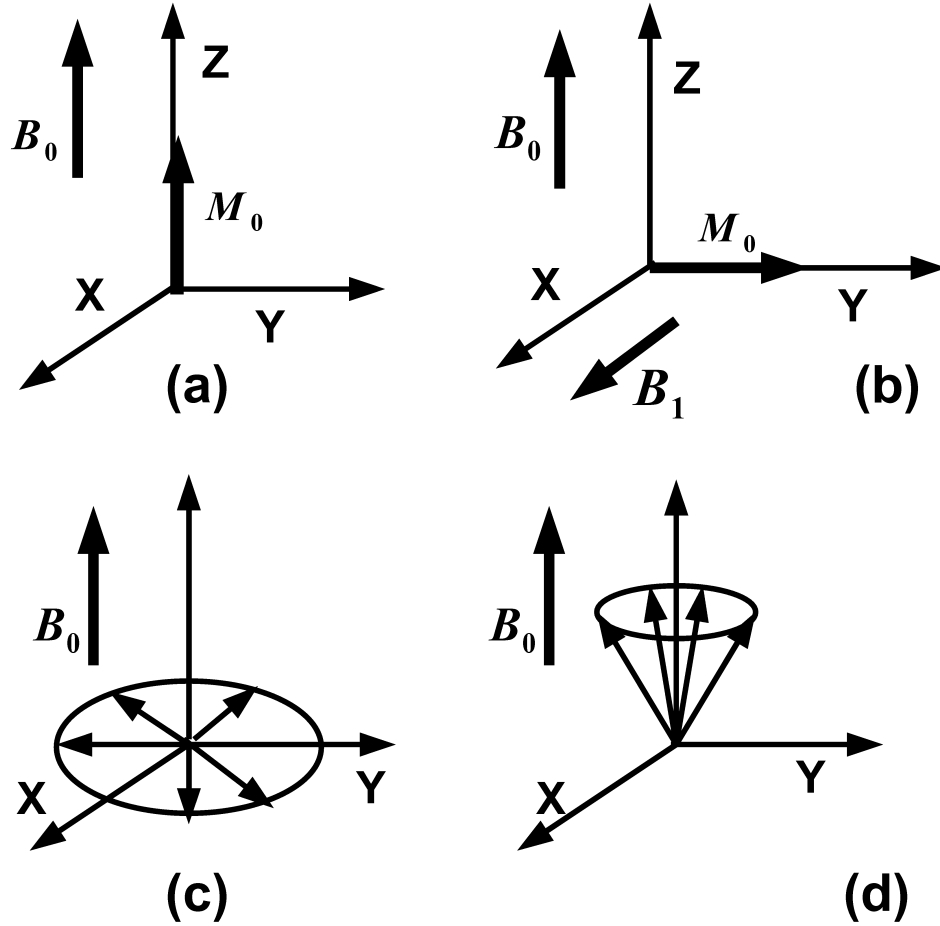
Figure 3.2: (a) Magnetization vector pointing along the direction of applied gradient (b) An oscillatory pulse rotates the magnetization into ZY plane (c) In the rotating frame, local variation in Larmor frequency give rise to dephasing of magnetization (d) Magnetization approaches the equilibrium state.
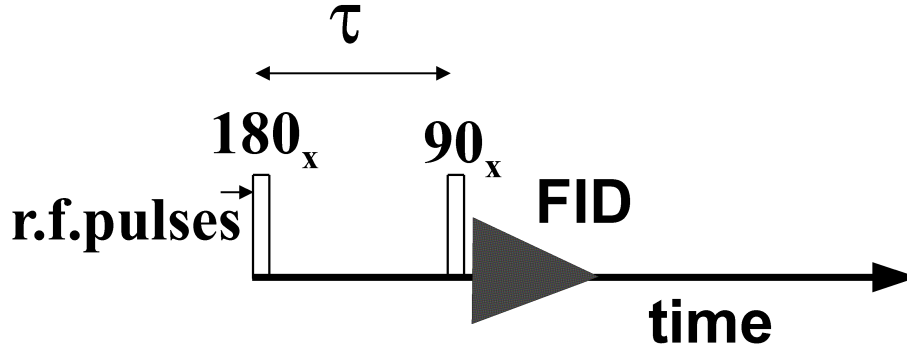
Figure 3.3: Inversion recovery pulse sequence.

3.2.2 Spin-spin Interaction

The 'spin echo' (Figure 3.4) can be used to measure the time constant T_2 for spin-spin relaxation. There are two mechanisms that give rise to broadening of NMR peaks: homogeneous and inhomogeneous broadening. Homogeneous broadening arises from the spin-spin interaction (fluctuation of local magnetic fields). Inhomogeneous broadening arises from variation of macroscopic magnetic fields due to sample imperfection or susceptibility inhomogeneities (or because of B_0 field uniformity, in spite of shimming, is never perfect).

Here a 90^0 pulse is first applied to the spin system. The 90^0 degree pulse rotates the magnetization down into the XY plane. The transverse magnetization begins to dephase. At some point in time after the 90^0 pulse, at time $\tau/2$ a 180^0 pulse is applied. The 180^0 pulse in the spin echo inverts the inhomogeneous part of the signal decay. Thus in the absence of T_2 relaxation, there is at time τ, an 'echo' of the FID. In the presence of spin-spin interaction, the echo is attenuated exponentially with a time constant T_2. In this case a signal can be written as

$$S \propto (\exp(-\tau/T_2)) \tag{3.3}$$
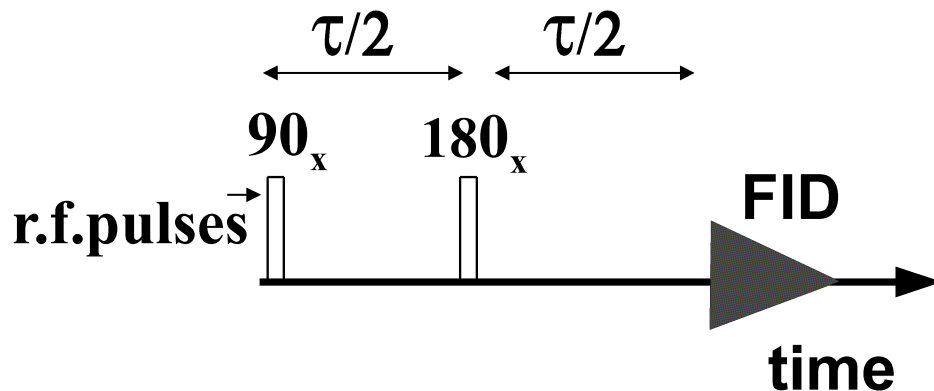
which is an exponential decay.

Figure 3.4: Spin echo pulse sequence.

3.3 NMR Interactions

In general the nucleus interacts with its environment because it has electric charges (which interact with an electric field) and it may have a magnetic moment (which interacts with a magnetic field). Some of the interactions are presented here.

3.3.1 Chemical Shift

There is a magnetic interaction between an external magnetic field and the nuclear spins. The external magnetic field causes an induced magnetic field in the electron cloud. So the nuclear spins feel a local magnetic field which is the combination of the external as well as the induced magnetic field. But the electrons have different chemical environments at different sites. So there is a local variation of the magnetic field. In the case of a simple liquid like p-xylene (C_6H_4-$(CH_3)_2$), due to the difference in chemical environment, protons located in the -C_6H_4 groups experiences sightly different magnetic fields than the protons of -$(CH_3)_2$ groups. This is known as chemical shift. 1D NMR Spectra of ethanol is shown in Figure 3.5.

3.3.2 Quadrupole Coupling

In the case of nuclear spin greater than $1/2$, the electric quadrupole moment of the nucleus interacts strongly with the electric field gradients generated by the surrounding electron clouds. The quadrupolar coupling is a predominant
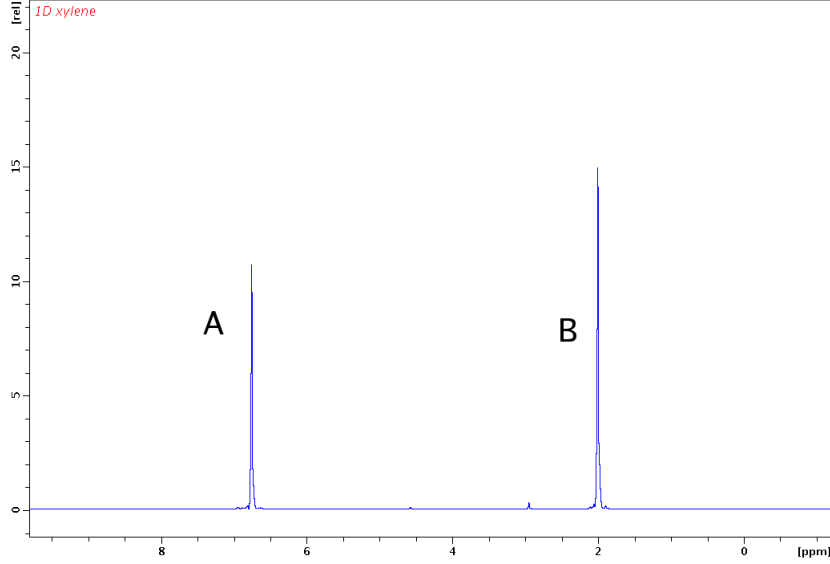
Figure 3.5: 1D NMR Spectra of p-xylene. Here A and B are the phenyl (C_6H_4) and methyl (CH_3) peaks respectively.

intermolecular interaction. For isotopic liquid quadrupole coupling averages to zero while it has a finite contribution in the case of liquid crystal [59]. In this thesis, the NMR-active nucleus is the proton (^{1}H, spin $\frac{1}{2}$) therefore quadrupolar coupling is not relevant.

3.3.3 Direct Dipole-Dipole Coupling

Dipole-dipole coupling is the direct magnetic interaction of nuclear spins with each other. Since each nuclear spin is magnetic, it generates a magnetic field which interacts with that of other nuclear spins. The interaction is known as direct dipole-dipole coupling because the fields between the nuclear spins propagate without involving the electron clouds. Figure 3.6 shows the dipole-dipole interaction between two nuclear spins i and j in the presence of the static magnetic field B_0. The interaction potential is

$$V_{dd}(\theta) \propto \frac{1}{r^3}(3\cos^2\theta - 1) \tag{3.4}$$

Here θ is the angle between internuclear vector and the static field. r is the distance between the nuclear spins i and j. In the case of liquids, due to rapid motion of molecules $\langle 3\cos^2\theta - 1 \rangle = 0$. But for solid and anisotropic liquid, dipole-dipole coupling causes pulse broadening. The dipole-dipole coupling
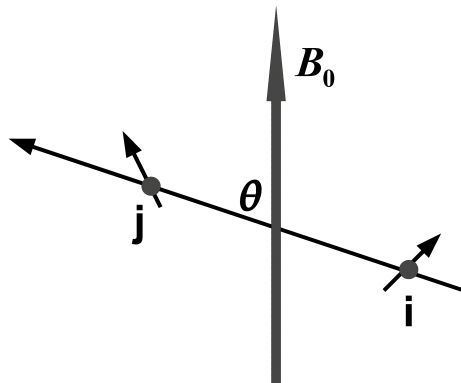
29

Figure 3.6: Dipole-dipole interaction.

may be either intramolecular or intermolecular. It is an interaction through space.

3.3.4 J-coupling

J-coupling is an indirect magnetic interaction of nuclear spins with each other, through the involvement of the electrons. The chemical shift indicates the local electronic environment while J-coupling provides the information about the chemical bond. The J-coupling is exclusively intramolecular.

3.4 NMR and Translational Motion

In the description of a one-dimensional single-pulse experiment, both B_0 and ω_0 are homogeneous throughout the system. If in addition to B_0 there is a spatially dependent magnetic field gradient g, the Larmor frequency becomes spatially dependent and

$$\omega = \gamma B_0 + \gamma g z \tag{3.5}$$

The phase shift in the time interval t is given by

$$\phi(t) = \gamma B_0 t + \gamma \int_0^t g(t')z(t') \, dt' \tag{3.6}$$

The dephasing due to the gradient pulse is a function of the gyromagnetic ratio of the nucleus and gradient strength. So a magnetic field gradient can be used to label the position of the spins.
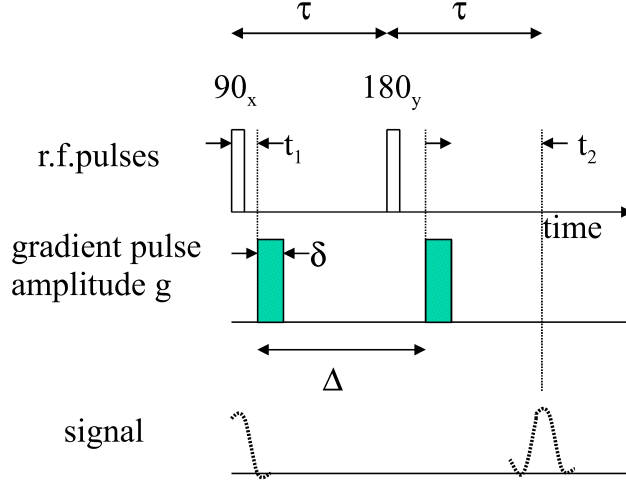
Figure 3.7: Pulsed field gradient spin echo pulse sequence.

3.4.1 Pulsed Field Gradient Spin Echo

As discussed earlier, in a spin echo pulse sequence the precessional phase shifts associated with the position of a molecule in a magnetic field gradient in time τ are exactly canceled at time 2τ by a 180^0 pulse that reverses the phase evolution giving rise to an echo of the FID. Any movement of molecule in this time scale causes an attenuation reduction of the echo signal. Both random and directed translational motion can be measured via a spin echo [60].

The mechanism of a spin echo pulse sequence with gradients (thus called the pulsed-gradient spin echo or PGSE experiment) is shown in Figure 3.7. A 90^0_x radio frequency pulse is applied which rotates the magnetization from the Z axis to XY plane. During the first τ period at time t_1 a gradient pulse of duration δ and magnitude g is applied. At the end of the first τ period, the phase shift is

$$\phi(\tau) = \gamma B_0 \tau + \gamma g \int_{t_1}^{t_1+\delta} z(t)\, dt \tag{3.7}$$

Here g has a constant amplitude over time. At the end of the first τ period, a 180^0_y rf pulse is applied which reverses the sign of the precession. At time $t_1 + \Delta$, a second gradient pulse of equal magnitude and duration is applied. If the spins have moved, the degree of dephasing is proportional to the displacement

31

in the direction of the gradient in the duration Δ. Now the total phase shift is given by [61]

$$
\begin{aligned}
\phi(2\tau) &= \left[\gamma B_0 \tau + \gamma g \int_{t_1}^{t_1+\delta} z(t)\,dt \right] - \left[\gamma B_0 \tau + \gamma g \int_{t_1+\Delta}^{t_1+\Delta+\delta} z(t')\,dt' \right] \\
&= \gamma g \left[\int_{t_1}^{t_1+\delta} z(t)\,dt - \int_{t_1+\Delta}^{t_1+\Delta+\delta} z(t')\,dt' \right]
\end{aligned}
\tag{3.8}
$$

The echo signal attenuation $S(\Delta, \delta, g)$ at $t = 2\tau$ can be written as [62]

$$
S(\Delta, \delta, g) = S_0 \int_{-\infty}^{\infty} P(\phi, 2\tau) \exp{(i\phi)} d\phi
\tag{3.9}
$$

where S_0 is the signal in the absence of a field gradient. $P(\phi, 2\tau)$ is the phase distribution function. Since for randomly varying quantities (as in diffusion), the phase distribution function is given by a normalized gaussian function, the signal can be written as

$$
S(g) = S_0 \langle \exp{(i\Delta\phi)} \rangle = S_0 \langle \exp{\frac{-(\Delta\phi)^2}{2}} \rangle
\tag{3.10}
$$

In the short gradient pulse limit (the SGP approximation), i.e., when $\delta \ll \Delta$, this equation can be written as

$$
S(g) = S_0 \exp{(-\gamma^2 g^2 \delta^2 D(\Delta - \delta/3))}
\tag{3.11}
$$

where D is the self diffusion coefficient. Therefore in a pulsed-field-gradient experiment, one can vary a generalized gradient strength parameter k, where k$= \gamma^2 g^2 \delta^2 (\Delta - \delta/3)$.

Observation of the signal attenuation with increasing k yields the self-diffusion coefficient.

For the system in which we are interested, the spin-spin relaxation is very short which causes a severe restriction on diffusion time Δ . This is because there is a second term in the attenuation equation

$$
S(g) = S_0 \exp{(-\gamma^2 g^2 \delta^2 D(\Delta - \delta/3))} \exp{(\frac{-\Delta}{T_2})}
\tag{3.12}
$$

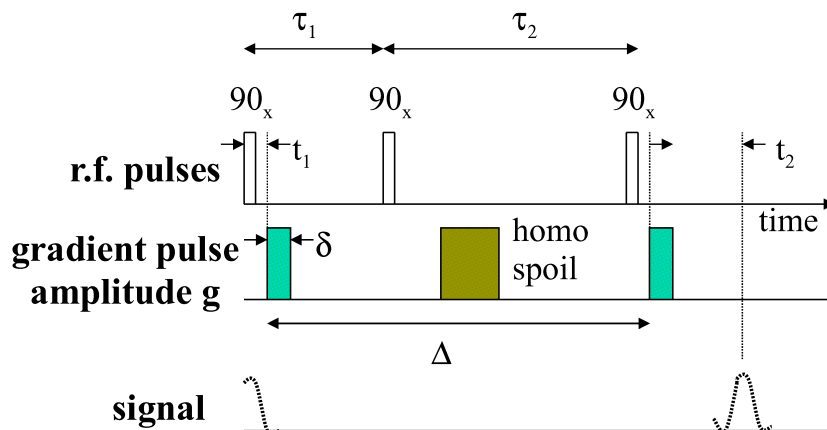So we use a stimulated echo pulse sequence (Figure 3.8).

Figure 3.8: Pulsed field gradient stimulated echo pulse sequence.

3.4.2 Pulsed Field Gradient Stimulated Echo

In the stimulated echo pulse sequence (Figure 3.8), the 180^0 pulse is replaced by two 90^0 pulses separated by a time interval τ_2 (also known sometimes as the storage time since the coherence is 'stored' along the Z axis) much longer than the first time interval τ_1. After the second 90^0 pulse a homospoil gradient is applied to kill the remnants of transverse magnetization.

The diffusion time in this experiment is determined by the largest time which is τ_2 and echo signal attenuation due to spin relaxation is determined by T_1. So the stimulated echo pulse sequence is well suited to measure slow diffusion. In all samples we study, T_1 is much longer than T_2.

3.5 PFG NMR of Colloidal suspension

A molecule having different chemical species has different individual chemical shifts. A liquid sample containing different molecular species will thus containing chemical shifts for each chemical group of each molecule. We can easily trace the particle motion just by observing the echo attenuation of these peaks in a pulsed-field gradient spin echo experiment. By this process, the diffusion coefficient for different chemical species can be measured simultaneously in the same experiment. In a single sentence, the advantage of a PFG NMR study would be to obtain spectrally resolved diffusion coefficients.

33

But in solids, due to slowness of molecular motion, dipole-dipole interactions are not averaged out. Because of that ^{1}H NMR spectra have the linewidths of tens of kHz. Due to this, the accuracy of gradient labeling of spatial position gets poor and, as a result, the PFG NMR technique proves inefficient [63]. That is the reason why researchers rarely look at the dynamics of colloidal microspheres using NMR.

Wassenius et al [30] have carried out studies of core-shell latex particles using the pulsed field gradient spin-echo technique. They measured the restricted diffusion of oil in the particle cavity. However, no detailed studies of colloidal phase behavior have been carried out by PFG NMR. In these experiments colloids had uncontrolled and large polydispersities.

In the experimental section, we will discuss our method of designing a colloidal model system for PFG-NMR studies of colloidal phase transitions.

Chapter 4

EXPERIMENTAL METHODS

One of the primary results presented in this thesis is the synthesis of a colloidal model system for NMR studies. We modified commercial monodisperse colloidal spheres to be visible both by NMR spectroscopy and fluorescence laser-scanning confocal microscopy. Methods for this colloid synthesis as well as sample preparation techniques are discussed here.

4.1 Preparation of NMR Visible, Fluorescent Colloids

Our primary goal was to synthesize fluorescent-labeled particles that could be studied both by NMR and confocal microscopy. Solid polystyrene has a broad peak width and extremely short relaxation times. It is thus unobservable in standard high-resolution NMR spin echo or stimulated echo experiments. Since the purchased colloidal particles were not fluorescent labeled, we added a fluorescent dye dissolved in an organic liquid. The organic liquid ('oil') made the colloidal particle NMR-visible while fluorescent dye made the particle visible by laser scanning microscopy.

The diffusion time (Δ) is a control parameter in pulsed-field gradient NMR experiments. For short diffusion times, oil diffuses inside of a polystyrene matrix and the diffusion coefficient represents the oil diffusion in an infinite porous polystyrene medium. For long diffusion times the diffusion of oil represents the diffusion of the particle itself which is the quantity we wish to measure. Figure 4.1 shows a schematic view of the diffusion of oil and particle.
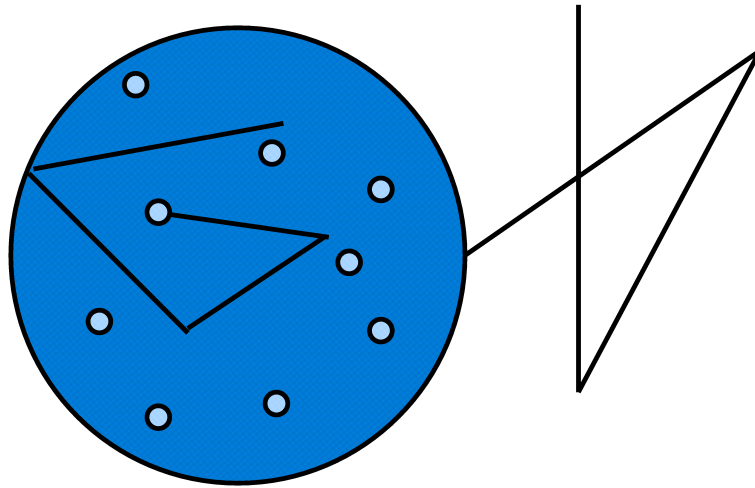
Figure 4.1: Cartoon of random motion of oil droplets inside a colloidal polystyrene (PS) particle. For short diffusion time, one observes diffusion of oil in the PS matrix. For long time (corresponding to multiple passes of the oil droplet between the walls) one begins to measure diffusion of the colloidal particles itself.

Table 4.1: Particles Description

Catalog Code	Mean Diameter(μm)	Lot Number
PS03N	0.99 ± 0.1	5750
PS03N	0.79 ± 0.03	6754
PS03N	0.54 ± 0.05	5702
PS02N	0.25 ± 0.04	7307

4.1.1 Characterization of Bare Particles

Polystyrene of different mean diameters (0.99 μm, 0.79 μm, 0.54 μm and 0.25 μm) were purchased from Bangs Laboratories, Inc. We measured the size distribution of all particles via scanning electron microscopy (SEM). SEM images are shown in Figure 4.2. A description of all particles are presented in Table 4.1. Here 0.99 μm particles have 10% polydispersity (measured from Figure 4.2(A)), while the rest have polydispersity of 5% or below. This difference in polydispersity is seen both in the images shown (Figure 4.2(A) and (C)) and in the distibution (Figure 4.2(B) and (D)). All of these particles are in a suspension of deionized water and 0.1% sodium dodecyl sulfate (SDS) which is a surfactant.
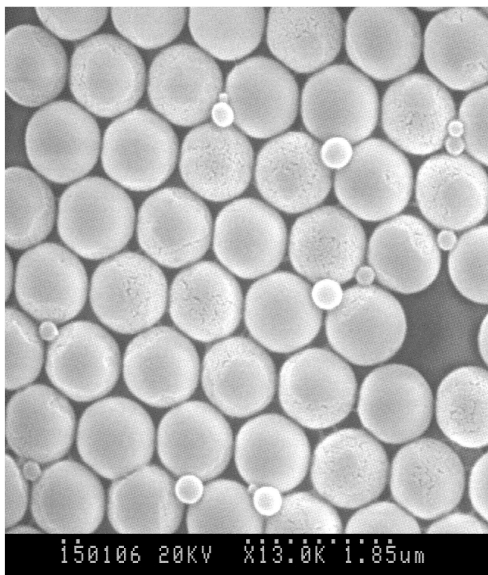
The volume fraction (ϕ) of stock colloidal solution was determined by analysis of the dry weight of a small sample. 50 μl of suspension was transferred in an aluminum paper of known mass using a pipette. We used a pipette of Fisherbrand Finnpipette II that covers a volume range from 20 μl to 200 μl. The plate was kept at 50^0C in an oven (Fisher Isotemp 500 series) for four hours. By that time only the dry polystyrene colloids were left in the plate. We used a scale (Mettler AF260 Deltarange) to measure the mass of dried polystyrene to a precision of 0.0001 gm. The volume of the polystyrenes (V_{PS}) was calculated from the density which is 1.05 gm/cm^3. Then the volume fraction (ϕ) was measured by using

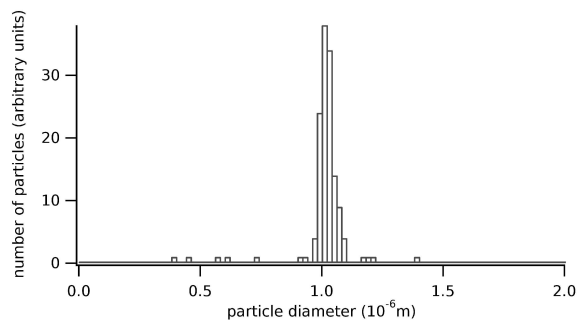$$\phi = V_{PS} \div 50 \ \mu l \times 100 \ \%$$

By this process the volume fraction of particles of four different diameters were measured as given in Table 4.2.
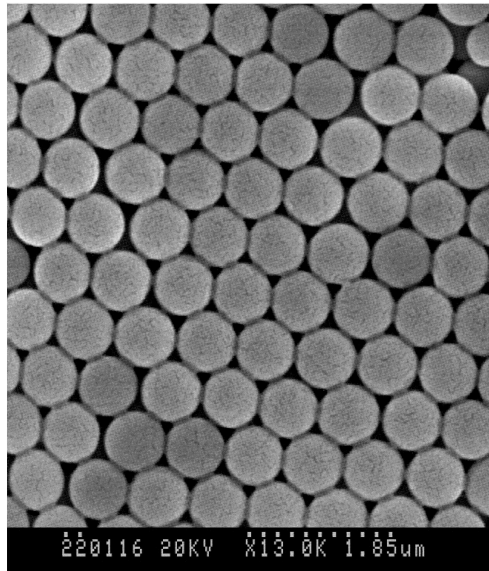
4.1.2 Preparation of Oil-Infused Colloids

Several solvents were tested to find ones that simultaneously satisfied the following criteria: (1) Solubility of fluorescent dye in it (2) insoluble in water
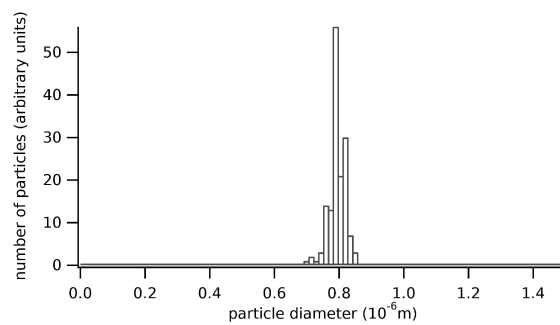
(A)

(B)

(C)

(D)

Figure 4.2: SEM images and analysis of size distribution for 0.99 μm spheres (Figure A and B) and for 0.79 μm spheres (Figure C and D). Here 0.99 μm particles have 10% polydispersity (measured from Figure 4.2(A)), while the rest have polydispersity of 5% or below.

Table 4.2: Volume fraction measurement

Mean Diameter(μm)	Volume Fraction
0.99	$(10.9 \pm 0.3)\%$
0.79	$(30.4 \pm 0.7)\%$
0.54	$(10.6 \pm 0.2)\%$
0.25	$(9.5 \pm 0.2)\%$

(3) Compatibility with polystyrene. The two solvents selected were p-xylene ('xylene') and tri-methyl phenyl silane ('TPS'), both of which satisfied the above criteria. P-xylene has a boiling point and density of 138^0C and 0.86 g/cm^3 respectively. In the case of tri-methyl phenyl silane boiling point and density are 170^0C and 0.87 g/cm^3. The reason for choosing oils of high boiling point was to avoid evaporation. We purchased p-xylene from Fisher (Product number: 05082-4, UN 1307, Class 1C) and tri-methyl phenyl silane from Sigma-Aldrich (Product Number: 79268, purum $\geq$ 98% GC). Fluorescent dyes we used are Coumarin 6 (98%, Product number: 442631, 1G) and Nile Red (Product number: N3013, 100mg), both purchased from Sigma Aldrich. Equal amount of (1 cm^3) of colloidal suspension for each particle size were transferred into different glass vials (Fisherbrand, 1 dram, 15 mm ϕ × 45 mm). Again we used a pipette of Fisherbrand Finnpipette II that covers a volume range from 200 μl to 1000 μl.

A solution of fluorescent dye dissolved in either xylene or TPS (referred to in the following discussion simply as 'oil') was prepared. An amount of this solution corresponding to 50% of the total volume of spheres was added to each colloidal suspension. For example in the case of a 1 cm^3 solution of 0.99 μm spheres in water, the total volume occupied by the spheres was (10.9% of 1 cm^3) equal to 0.109 cm^3. So, 50% of the total volume of spheres (50% of 0.109 cm^3), equal to 54.5 μl oil was added to this suspension. After adding oil, the mixture of polystyrene and oil was ultrasonicated (Branson B8510-DTH) to break up the oil droplets and to promote speedy absorption into polystyrene matrix. Both the sonication time and temperature was different for samples of xylene and TPS. For all samples with xylene, the sonication time was 25 minutes and the solution temperature was 23^0C. On the other hand, for the samples of TPS, sonication time and solution temperature were 40 minutes and 30^0C respectively. The mixture was shaken by hand twice during ultrasonication. Eventually the oil was completely absorbed by the
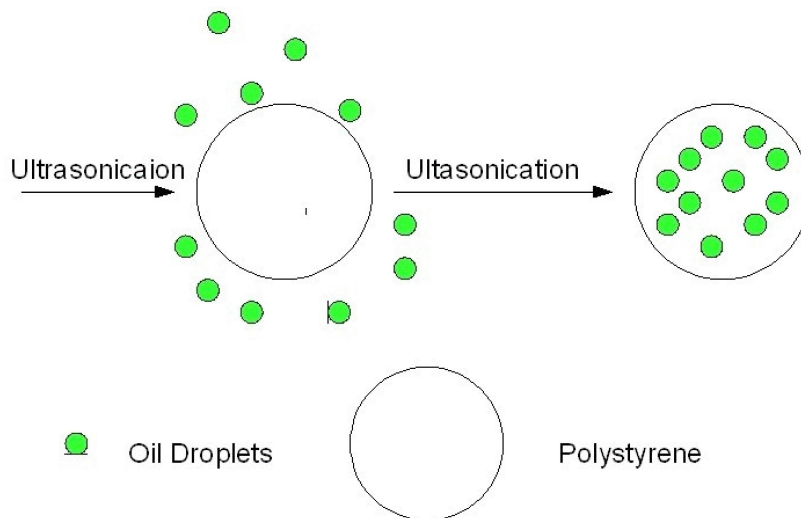
Figure 4.3: Schematic diagram of sample preparation.

spheres. The time needed for ultrasonication appeared also to vary with particle volume fraction. For example, ultrasonication time needed for samples with $\phi = 30\%$ was much smaller. However, it appears that short ultrasonication times also result in short T_2 relaxation times (discussed in Chapter 5). Figure 4.3 shows a schematic of the preparation technique.

So far we have discussed the synthesis of oil-infused particles for a volume fraction $\approx 10\%$. Now we will discuss the preparation of binary mixture of 0.99 μm and 0.79 μm spheres. 0.79 μm of colloid-water suspension (particle volume fraction= 30.4%) was transferred into a glass vial of 1 dram. The glass vial had 1 cm^3 of this suspension. P-xylene was added at 50% of the total volume of spheres. At 23^{0}C, after the ultrasonication for 5 minutes, we got oily spheres. Then water was added to get the volume faction of 21.3%.

We also made 0.99 μm sample for a volume fraction $\approx 22\%$. For this reason 5 cm^3 suspension of 0.99 μm colloids was taken in a 15 cm^3 disposable centrifuge tube (Fisher Scientific, Cat no: 05-539-5). Then the suspension was centrifuged (Sorvall centrifuge Legend MACH 1.6). The centrifuge speed was 800 rev/min. After 10 hours of centrifugation supernatant water was removed. By using dry weight of the sample, 22.4% particle volume fraction was obtained. 1 cm^3 of this suspension was transferred into a 1 dram glass
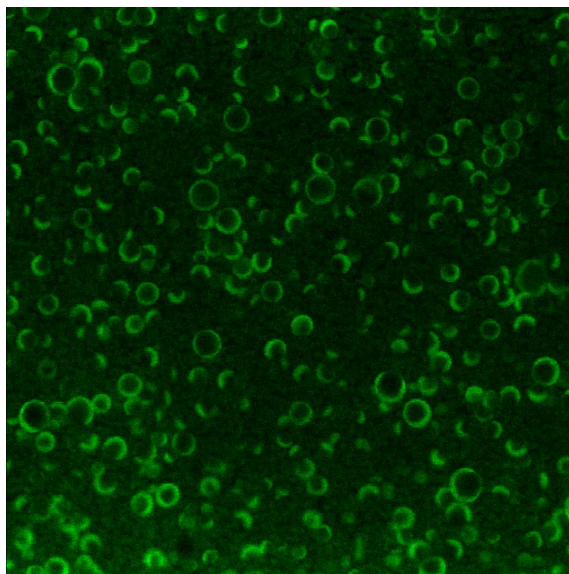
Figure 4.4: Confocal image of 0.99 μm spheres with the fluorescent dye (and p-xylene) not incorporated into the particles. In this case more ultrasonication is needed.
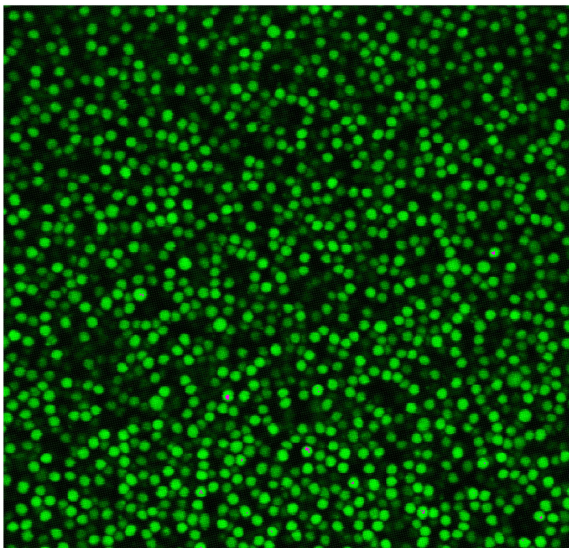

Figure 4.5: Confocal image of 0.99 μm spheres with the fluorescent dye (and p-xylene) inside the particles.

Table 4.3: List of Samples Prepared

Samples(μm)	Volume Fraction	Sonication Time	Temp.
0.99μm (p-xylene)	(10.9 $\pm$ 0.4)%	25 min	23^{0}C
0.99μm (tri-methyl phenyl silane)	(10.9 $\pm$ 0.3)%	40 min	30 ^{0}C
0.79μm (p-xylene)	(11.9 $\pm$ 0.5)%	25 min	23^{0}C
0.54μm (p-xylene)	(10.6 $\pm$ 0.3)%	25 min	23^{0}C
0.25μm (p-xylene)	(9.5 $\pm$ 0.2)%	25 min	23^{0}C
Binary Mixture:			
0.99μm(tri-methyl phenyl silane)	(22.4 $\pm$ 0.5)%	5 min	30^{0}C
0.79μm(p-xylene)	(21.3 $\pm$ 0.3)%	5 min	23^{0}C

vial and tri-methyl phenyl silane was added at 50% of the total volume of spheres. 5 minutes of ultrasonication at 30^{0}C was enough for the oil to go inside the spheres.

Now 3 cm^3 suspension of 0.99 μm ($\phi = 22.4\%$, tri-methyl phenyl silane inside) was added with the same volume amount of 0.79 μm suspension ($\phi = 21.3\%$, p-xylene inside). Hence we prepared the binary mixture of two different size particles with different oils inside. Table 4.3 shows the list of all samples.

The fluorescent dye dissolved in the oil made the colloids fluorescent-labeled and thus could be viewed by confocal microscopy. In this way we could confirm that the oil was absorbed by the polystyrene spheres. For example, Figure 4.4 shows a confocal image of 0.99 μm spheres with the fluorescent dye (and p-xylene) not incorporated into the particles while in Figure 4.5 fluorescent dye (and p-xylene) incorporated into the particles. Thus this technique simultaneously makes cheap fluorescent-labeled colloids as well as NMR visible colloids. We transferred the all samples in 7 inch length round bottom NMR tubes manufactured by Norell, Inc. The sample heights in each tubes were 4.5 to 5 cm.

4.2 Conductivity Characterization of Colloid Interactions

We confirmed our spheres behave like hard spheres just by measuring solvent conductivity. We used a multi-function conductivity meter (Amber Science Inc., Model 3082 series). It had two types of cells known as a dip cell and

Table 4.4: Values of κa for the suspension of different size spheres

Mean Diameter(μm)	Conductivity(mS/cm)	κa
0.99	2.86 ± 0.04	231
0.79	2.86 ± 0.08	185
0.54	2.86 ± 0.03	126
0.25	2.86 ± 0.03	58

a flow cell. Conductivity cells usually consist of two metallic plates of a determined size mounted in a defined area. The cell constant 'K' (K=L/A) is the ratio of the distance between the plates (L) of the conducting path in centimeters to effective cross sectional area (A) of the conducting path in square centimeters. This model was designed to use a cell with a constant of 10 cm^{-1}. We measured conductivity of all samples using a dip cell. The value of conductivity was 2.86 ± 0.04 mS/cm (note 1 S = 1 Ω^{-1}). This was equivalent to the concentration of Potassium Chloride (KCl) of 2.02 $\times 10^{-2}$ mole/liter in pure water. Then by using Equation 1.4, we obtained a value for κ^{-1} which was 2 nm. Table 4.4 shows κa for different particles. We considered a system to be a nearly hard sphere system when the dimensionless parameter $\kappa a \geq 10$. All dilutions of colloidal suspensions used potassium chloride (KCl) in water solutions in order to keep the Debye-Hückel length small. For example before adding oil, the suspension of 0.79 μm spheres was diluted with the solution of potassium chloride (KCl) in water (which had the conductivity of 2.86 mS/cm).

4.3 PFG NMR Measurements

PFG-NMR measurements were carried out on a Bruker Avance II 600 spectrometer equipped with a Bruker 14.08 T magnet, Bruker diffusion probe known as Diff30. The Diff30 probe had a Z gradient strength of 30 G/cm/A. The spectrometer was also equipped with a gradient amplifier of 60 Amp maximum current. So the maximum gradient was 1800 G/cm (18 T/m) by which we could measure the diffusion coefficient on the order of 10^{-15} m^2/s. To avoid heating and to keep a constant sample temperature throughout the experiment, the probe was cooled by flowing water. A temperature control unit, known as BTU, was used for this purpose. The probe also includes exchangeable rf coil inserts with various inner diameters and resonance fre-

quencies. As we were observing magnetic resonance of the ^{1}H nucleus (proton NMR), the radiofrequency (rf) coil for ^{1}H was used which had an inner diameter of 5 mm.

In the beginning of every experimental slot, we replaced the existing probes, and inserted the Diff30 probe. Then we connected the gradient cable and two tubes (one for water IN and another for water OUT) with it. Switching BTU on allowed the water to circulate inside the probe. We had to gently turn the probe upside down a few times to make sure that there were no air bubble inside the probe. Then we inserted the probe inside the magnet. As the control software (Topspin 1.3) is installed in Linux system, we had to connect the data server and console just by changing the cables. In the AQS/2 cabinet we had to confirm that the right cable (HZ04360) was connected. Then pushing the red button of AQS/2 would reset the system. Pressing the 'Reset' button of Gradient unit made the gradient probe active. When the change of probe was complete, we inserted our sample. Topspin software was used for further experimental setup. First we had to check that the software could recognize the probe. Then the next thing to check was sample temperature. We could change the sample temperature by using the software. Then we tuned the receiver manually to resonance with the oscillating magnetic field produced by Larmor precession of the nuclear spins in the sample. Homogeneity of the magnetic field is a very important issue for NMR experiments. In the jargon of NMR, this is known as 'shimming'. Poor shimming causes an inhomogeneous broadening of the NMR spectrum. As soon as we reached the target temperature of the sample, we shimmed on the fourier transform of FID (the NMR spectrum) to maximize peak intensity or minimize peak width. All experiments were done at 25^0C.

After the adjustment of temperature, tuning and shimming, we carried out experiments to select the duration P_1 for a 90^0 pulse for our samples. This was done by a series of experiments where the pulse duration P_1 was varied. For a value of P_1 corresponds to 360^0 pulse, signal intensity was zero. Dividing the 360^0 pulse time by 4, we measured the 90^0 pulse length. We then setup a one-dimensional (1D) experiment.

Figure 4.6 and Figure 4.7 show the fourier transformed 1D spectrum for p-xylene and tri-methyl phenyl silane inside 0.99 μm and 0.79 μm particles respectively. In both Figure 4.6 and Figure 4.7 the large peak (marked B) between 4 and 5 ppm is the water peak, and the peaks near 7 ppm (marked A) come from phenyl groups. The peaks marked C in Figure 4.6 and Figure 4.7, however at different chemical shifts, are methyl peak. The methyl
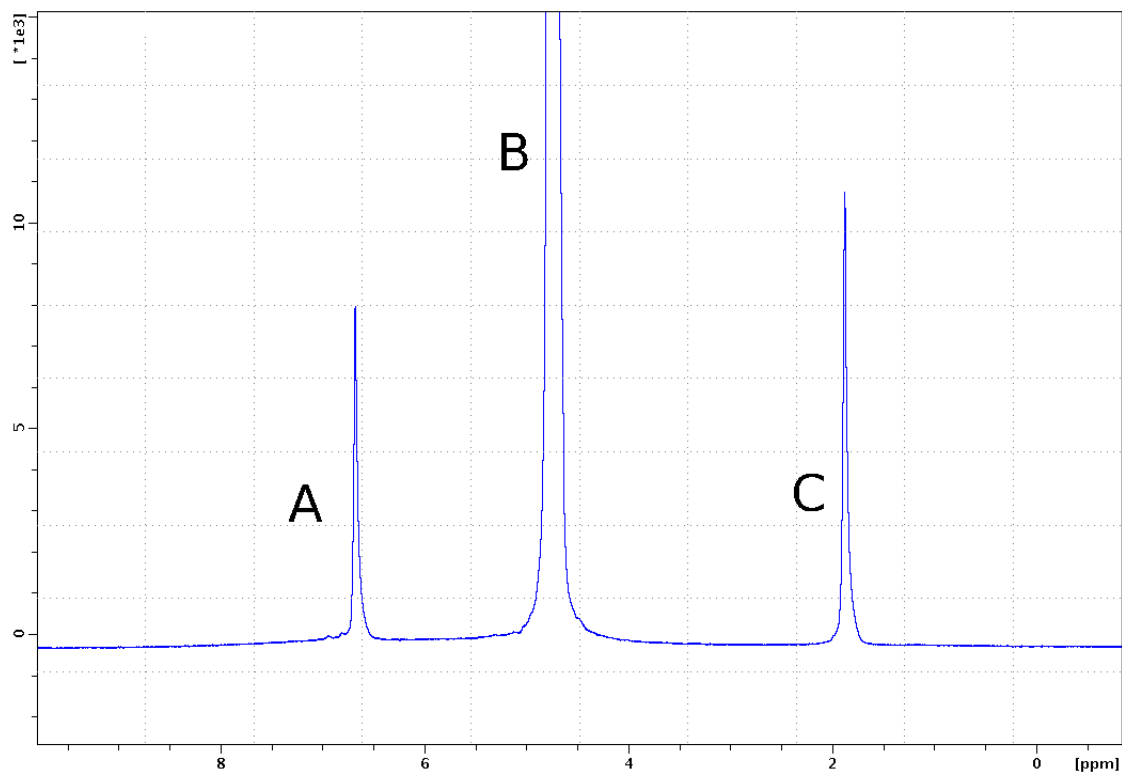
Figure 4.6: 1D spectrum of p-xylene inside 0.99 μm colloids. A, B and C are the phenyl, water and methyl peaks respectively.

peak in Colloid- 0.99 μm is shifted from the Colloid- 0.79 μm methyl peak by 2 ppm.

As discussed in Section 3.4.1 and Section 3.4.2, a stimulated echo pulse sequence was used to measure the diffusion coefficient. The parameters included $\Delta = 300$ ms, $\delta = 2$ ms and gradient values were varied according to the purpose of each experiment. The diffusion time Δ can be varied to probe short or long time diffusion, but was limited by signal strength (longer Δ causes more T_1 relaxation). The gradient application time δ was limited primarily by T_2 relaxation. Also the time between successive repetitions of the experiment (for signal averaging), d_1, was chosen to be large compared to the T_1 relaxation time ($d_1 \geq 5T_1$). So T_1 and T_2 were very important parameters for diffusion experiments.
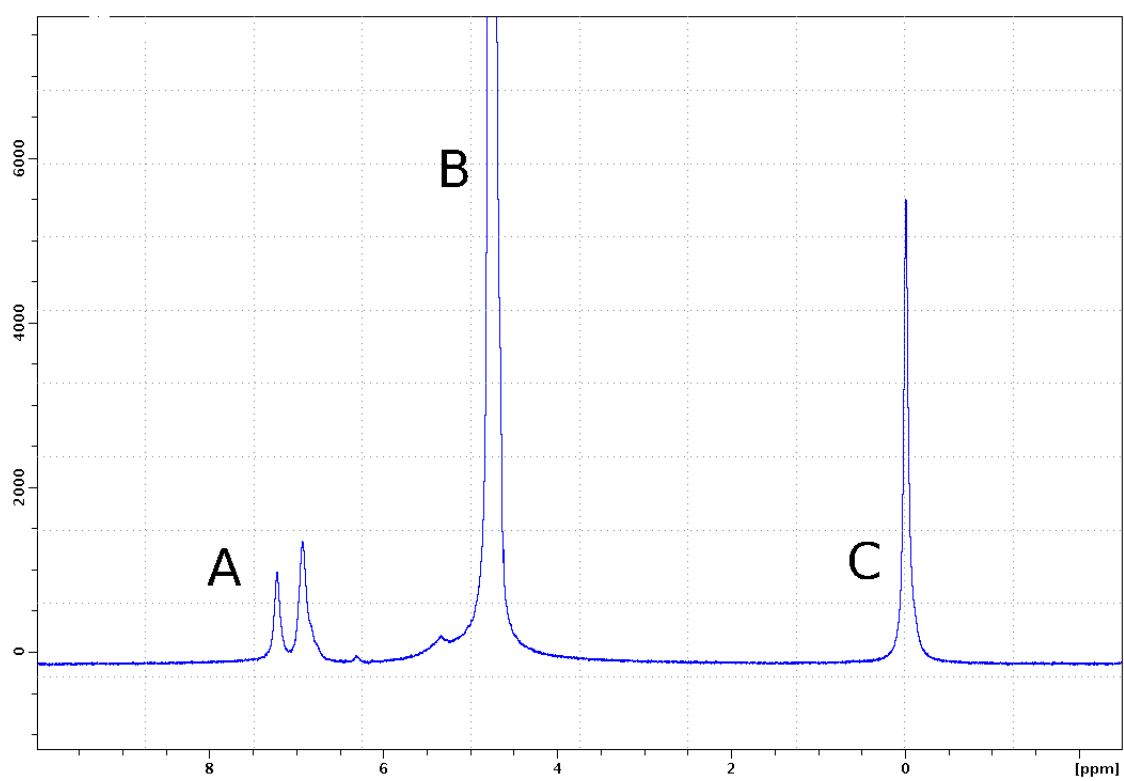
For each sample the list of NMR experiments we followed were:

45

Figure 4.7: 1D spectrum of tri-methyl phenyl silane inside 0.79 μm colloids. A, B and C are the phenyl, water and methyl peaks respectively.

- Determination of P_1.

- 1D experiment.

- T_1 and T_2 measurements.

- Diffusion experiment.

All experimental results are presented in the next chapter.

Chapter 5

RESULTS AND DISCUSSION

5.1 T_1 and T_2 Relaxation Times

We measured T_1 and T_2 for all samples by using the pulse programs described in Section 3.2.1 and Section 3.2.2. The results are shown in Table 5.1. The T_1 relaxation in all samples is of order 1 second. The T_2 relaxation varies widely from one sample to another between 90 ms and 200 ms. At the present time, it appears that longer T_2's correlate with longer ultrasonication times during colloid preparation. This is likely due to the fact that the oil slightly swells the polystyrene matrix. Longer ultrasonication might accelerate this process. It was also observed that the T_2 relaxation times measured immediately upon sample preparation was smaller than in the same sample a week later.

5.2   Diffusion Coefficient of Single Species

In monodisperse suspensions, one can obtain diffusion coefficients for the water peak and the methyl/phenyl peaks simultaneously. The signal attenuation of the water peak yields the water diffusion coefficient in the colloidal suspension according to the equation (from Equation 3.11)

$$S(g) = S_0 \exp\left(-\gamma^2 g^2 \delta^2 D(\Delta - \delta/3)\right) \tag{5.1}$$

Shown in Figure 5.1 is the signal attenuation for the p-xylene spectrum for gradient strengths (in G/cm) from 30 G/cm to 1000 G/cm in 32 steps where the water signal has been completely eliminated. This would not be the case for bulk p-xylene which has a self diffusion coefficient of the same order of magnitude as water ($\approx 2 \times 10^{-9}$ m^2/s). However, p-xylene in a polystyrene colloid diffuses more slowly ($\approx 1.4 \times 10^{-12}$ m^2/s).

Table 5.1: Relaxation times T_1 and T_2 for All Samples. The typical errors in T_1 was 0.1 s, T_2 was 0.2 ms.

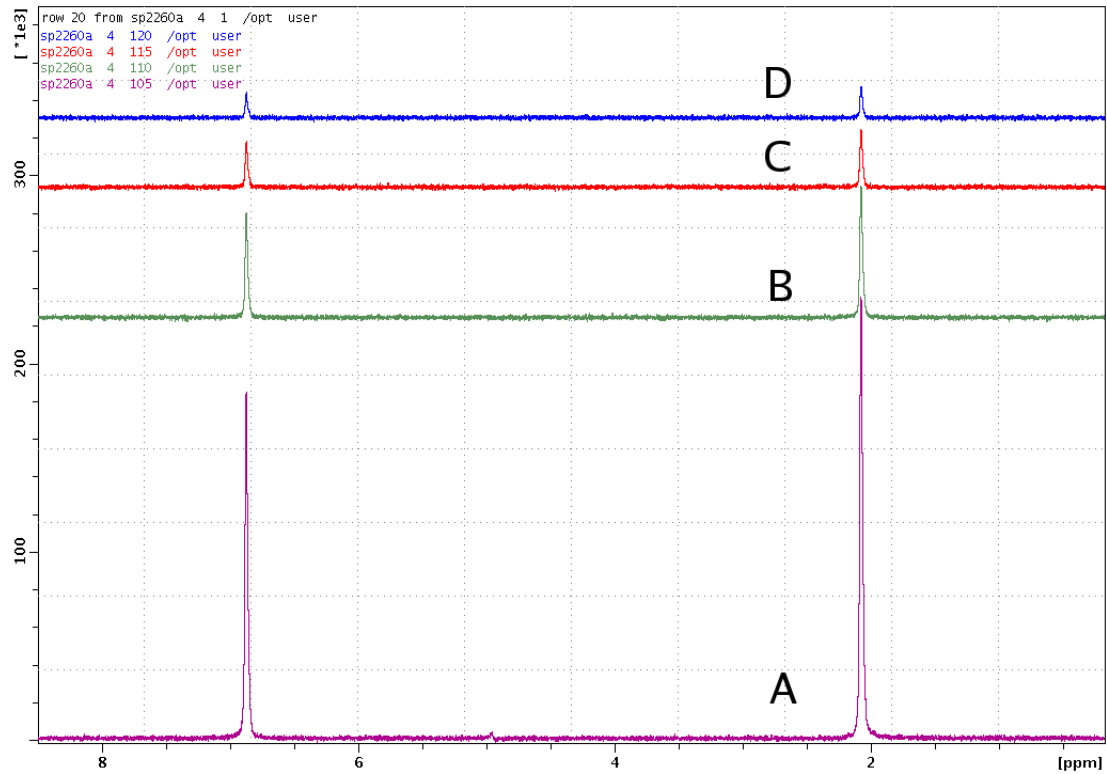| Samples(μm)	Volume Fraction	T_1	T_2.
0.99μm (p-xylene)	$(10.9 \pm 0.4)\%$	1 s	214.2 ms
0.99μm (tri-methyl phenyl silane)	$(10.9 \pm 0.3)\%$	1 s	147.6 ms
0.79μm (p-xylene)	$(11.9 \pm 0.5)\%$	1 s	96.7 ms
0.54μm (p-xylene)	$(10.6 \pm 0.3)\%$	800 ms	108.8 ms
0.25μm (p-xylene)	$(9.5 \pm 0.2)\%$	1 s	91.4 ms
Binary Mixture:			
0.99μm(tri-methyl phenyl silane)	$(22.4 \pm 0.5)\%$	1 s	92.0 ms
0.79μm(p-xylene)	$(21.3 \pm 0.3)\%$	1 s	108.5 ms

Figure 5.1: Stimulated echo signal attenuation of p-xylene signal for increasing gradient value (in gauss/cm) (A) 163.87 G/cm , (B) 318.71 G/cm, (C) 473.55 G/cm and (D) 628.399 G/cm.
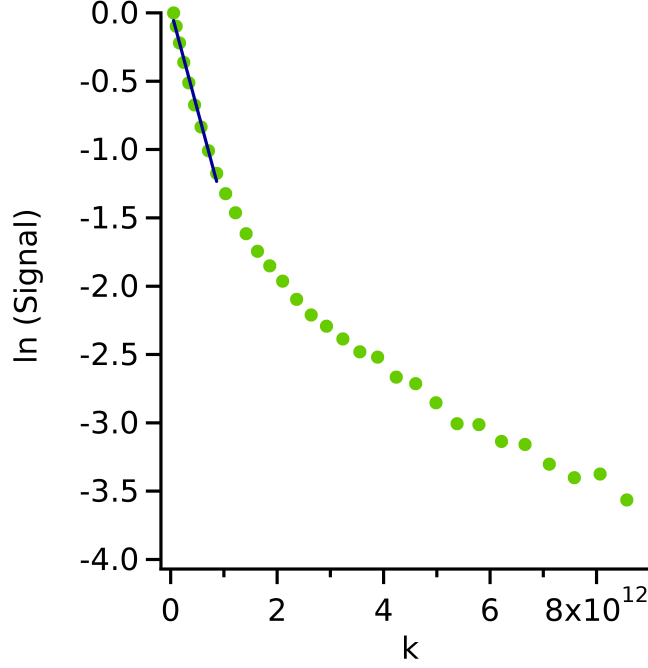
Figure 5.2: Non-mono-exponential signal attenuation curve for 0.99 μm polystyrene suspension. Note that ln(Signal) is plotted, so single exponential behavior according to Equation 5.1 would result in a linear plot. Here k is a gradient strength parameter where k= $\gamma^2 g^2 \delta^2 (\Delta - \delta/3)$. The initial slope $\approx 1.4 \times 10^{-12}$ m^2/s, is interpreted as the effective diffusion coefficient of p-xylene in the porous polystyrene matrix.

A signal attenuation for such an experiment is shown in Figure 5.2. Here the signal attenuation curve is not a mono-exponential curve. There are multiple effects that are important:

- P-xylene is diffusing in a porous polystyrene medium.

- We hypothesized that on exponential timescales, the porous medium simply makes the effective diffusion coefficient smaller.

- Even so, the p-xylene should see the effect of particle size (restricted diffusion).

- In addition, there is the slow diffusion of the colloid itself.

50

5.2.1 Restricted Diffusion

Diffusion of molecules inside a cavity is known as 'restricted diffusion'. As the molecules inside the cavity are not diffusing freely, the behavior of signal attenuation is different from that of unrestricted diffusion. Murday and Cotts [64] obtained the signal attenuation of a pulsed-field gradient spin echo experiment for the diffusion within a reflecting spherical boundary of radius a (note that this equation implies that the signal still has a mono-exponential dependence, but that the relation of the slope to the diffusion coefficient is more complicated)

$$S(g) = \exp\left(-2\gamma^2 g^2 F\right) \tag{5.2}$$

where $F = \sum_{m=1}^{\infty} f(\alpha_m)$ and

$$f(\alpha_m) = \alpha_m^2 (\alpha_m^2 a^2 - 2)^{-1} \left[\frac{2\delta}{\alpha_m^2 D} - \frac{2 + \exp\left(-\alpha_m^2 D(\Delta - \delta)\right) - 2\exp\left(-\alpha_m^2 D\delta\right)}{(\alpha_m^2 D)^2} \right. $$
$$\left. - \frac{2\exp\left(\alpha_m^2 D\Delta\right) + \exp\left(-\alpha_m^2 D(\Delta + \delta)\right)}{(\alpha_m^2 D)^2} \right] $$
$$\tag{5.3}$$

Here α_m are the roots of the Bessel function equation

$$\alpha_m a J'_{\frac{3}{2}}(\alpha_m a) - \frac{1}{2} J_{\frac{3}{2}}(\alpha_m a) = 0 \tag{5.4}$$

Still the signal attenuation for restricted diffusion is an exponential decay but apart from δ and Δ, it has a dependence on the size (a) of the cavity as well. Note that Equation 5.3 would reduce to the signal attenuation equation for bulk diffusion (Equation 5.1) when the size of the spherical boundary become very large. By using Mathematica we solved Equation 5.2 numerically for 2a= 0.99 μm, Δ= 300 ms, δ=2 ms and D= 1.4×10^{-12} m^2/s to 2×10^{-9} m^2/s. The dependence of F on D is shown in Figure 5.3.

Again a plot of signal attenuation of xylene inside 0.99 μm spheres is plotted as a function of k' where $k' = 2\gamma^2 g^2$. Following Equation 5.2, the slope of this exponential curve is equal to F. Figure 5.4 shows the plot where we obtained F= $(1.7 \pm 0.1) \times 10^{-18}$ m^2 s^2. From Figure 5.3 it is quite clear that there is no such value of F to get the diffusion coefficient of oil inside the particle. This is because the derivation of signal attenuation formula has been carried out only for the case of liquid contained in a spherical cavity.
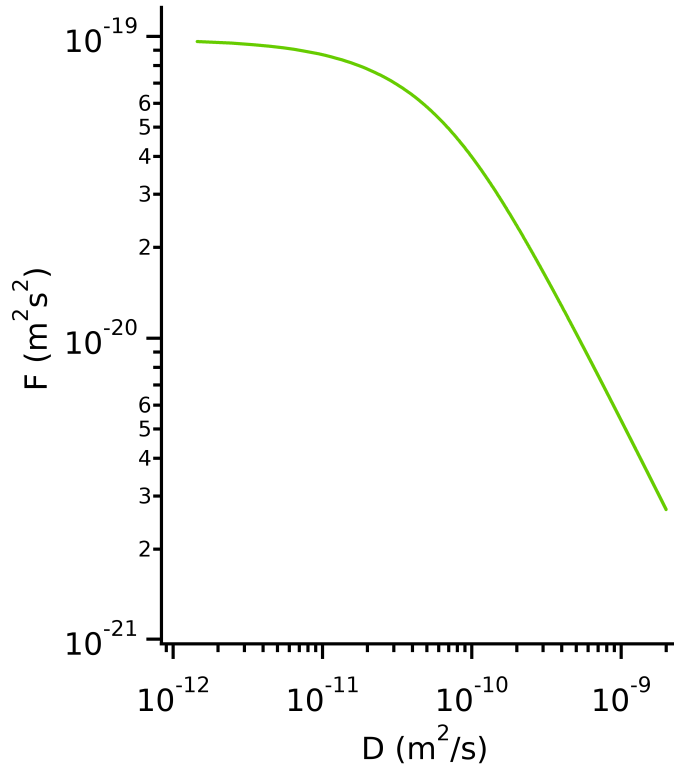
Figure 5.3: A numerical solution of Equation 5.3 for 2a= 0.99 μm, Δ= 300 ms, δ=2 ms and D= 1.4×10^{-12} m^2/s to 2×10^{-9} m^2/s. The range of D values used are experimentally reasonable values. The high value (2×10^{-9} m^2/s) is an upper limit corresponding to bulk p-xylene. The low value (1.4×10^{-12} m^2/s) get from initial slope of Figure 5.2.
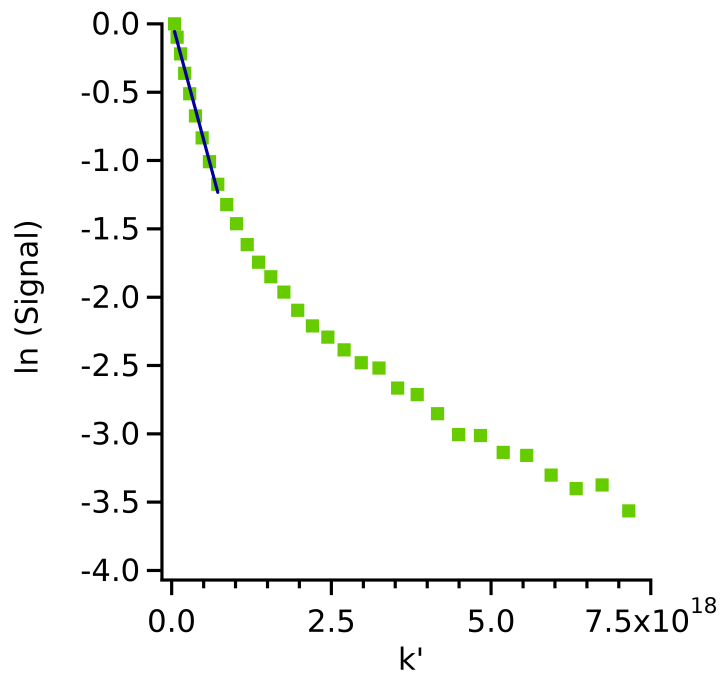
Figure 5.4: Signal attenuation curve for 0.99 μm polystyrene suspension as a function of k' where $k' = 2\gamma^2 g^2$. Here initial slope, F, is 1.7×10^{-18} m^2 s^2, should correspond to the low-gradient asymptotic value for effective xylene bulk diffusion in a polystyrene matrix.
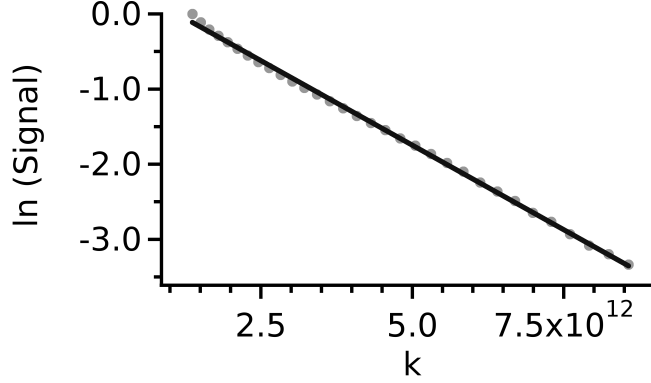
Figure 5.5: Experiments of large gradient show single slope behavior.

Thus our hypothesis that the porous medium simply made the effective diffusion coefficient smaller appears not to be valid. In the present case, we have oil diffusing within a polystyrene matrix which is a complex porous structure. Such diffusion in a porous structure can be simulated by using molecular dynamics simulation which has not done yet. So currently it is not possible to fit the entire data (for all gradient strengths) using a single functional form.

5.2.2 Relation of Diffusion Coefficient With Sphere Diameter

For all of our analysis, we assume reasonably that regardless of the final fit function for restricted diffusion, it should asymptotically approach the colloid diffusion value at large gradient strengths. It is shown in Figure 5.5 that the signal attenuation for large gradient show single slope behavior. Here the gradient strengths varied from from 300 G/cm to 1000 G/cm in 32 steps. Using the asymptote to the curve of ln (Signal) vs. gradient strength parameter k and for monodisperse colloidal suspensions with particle diameter 0.99 μm, 0.79 μm, 0.54 μm and 0.25 μm the diffusion measurement results are as shown in Table 5.2. It is worth mentioning that the diffusion coefficient for 0.99 μm colloids (for both xylene and TPS infused colloids) agrees, within error.

Figure 5.6 shows that our assumption (of asymptotic behavior at large gradients corresponding to colloid diffusion) for data analysis is indeed valid. The measured colloid diffusion values for different particle sizes are compared with

54

Table 5.2: Diffusion Coefficient of All Samples. In all cases we used the diffusion coefficient of HDO in pure D_2O (1.902×10^{-9} m^2/sec at 25^0C) as our calibration standard.

Samples(μm)	Diffusion Coefficient
0.99μm (p-xylene)	$(4.5 \pm 0.2) \times 10^{-13}$ m^2/sec
0.99μm (tri-methyl phenyl silane)	$(4.5 \pm 0.1) \times 10^{-13}$ m^2/sec
0.79μm (p-xylene)	$(3.3 \pm 0.1) \times 10^{-13}$ m^2/sec
0.54μm (p-xylene)	$(6.4 \pm 0.1) \times 10^{-13}$ m^2/sec
0.25μm (p-xylene)	$(1.3 \pm 0.4) \times 10^{-12}$ m^2/sec

the Stokes-Einstein prediction. The solid curve is for infinite dilution, while the dashed curve is the corrected functional form using hydrodynamic theory for a finite volume fraction of the suspensions. The diffusion coefficients measured are within $\approx 10\%$ of the theoretical value.

5.2.3 Comparison With Other Work

Comparing our data with other work done with PFG NMR [29, 30, 50], it is found that our results of diffusion coefficient agree quite well with the theoretical prediction. In an infinitely dilute suspension, the ratio D/D_0 is equal to 1. Because we did experiments for a finite volume fraction, D/D_0 should be less than 1 as shown in Figure 5.7. This ratio was far off for the experiment done by Wassenius et al [30], but is below unity in the experiments of Blees et al [29] and Wagner et al [50]. A value close to unity suggests that one is indeed probing true colloid diffusion.

5.2.4 Diffusion Coefficient For Different Diffusion Times

Free bulk diffusion would be characterized by independence of the diffusion coefficients obtained from the diffusion time Δ. Measuring the D vs Δ (Figure 5.8) we found that the diffusion coefficient decreases as ($A + B/\Delta$). Here A=$(6.13 \pm 0.02) \times 10^{-11}$ m^2/s and B=$(3.01 \pm 0.02) \times 10^{-13}$ m^2. Note B has the dimension (length)^2 and $\sqrt{B}$ corresponds to a length of 0.5 μm.

Our hypothesis for oil-infused particles was that for long enough Δ the diffusion of oil represents the diffusion of the particle itself. Figure 5.8 shows the dependence of diffusion coefficient on Δ. For a short diffusion time, the
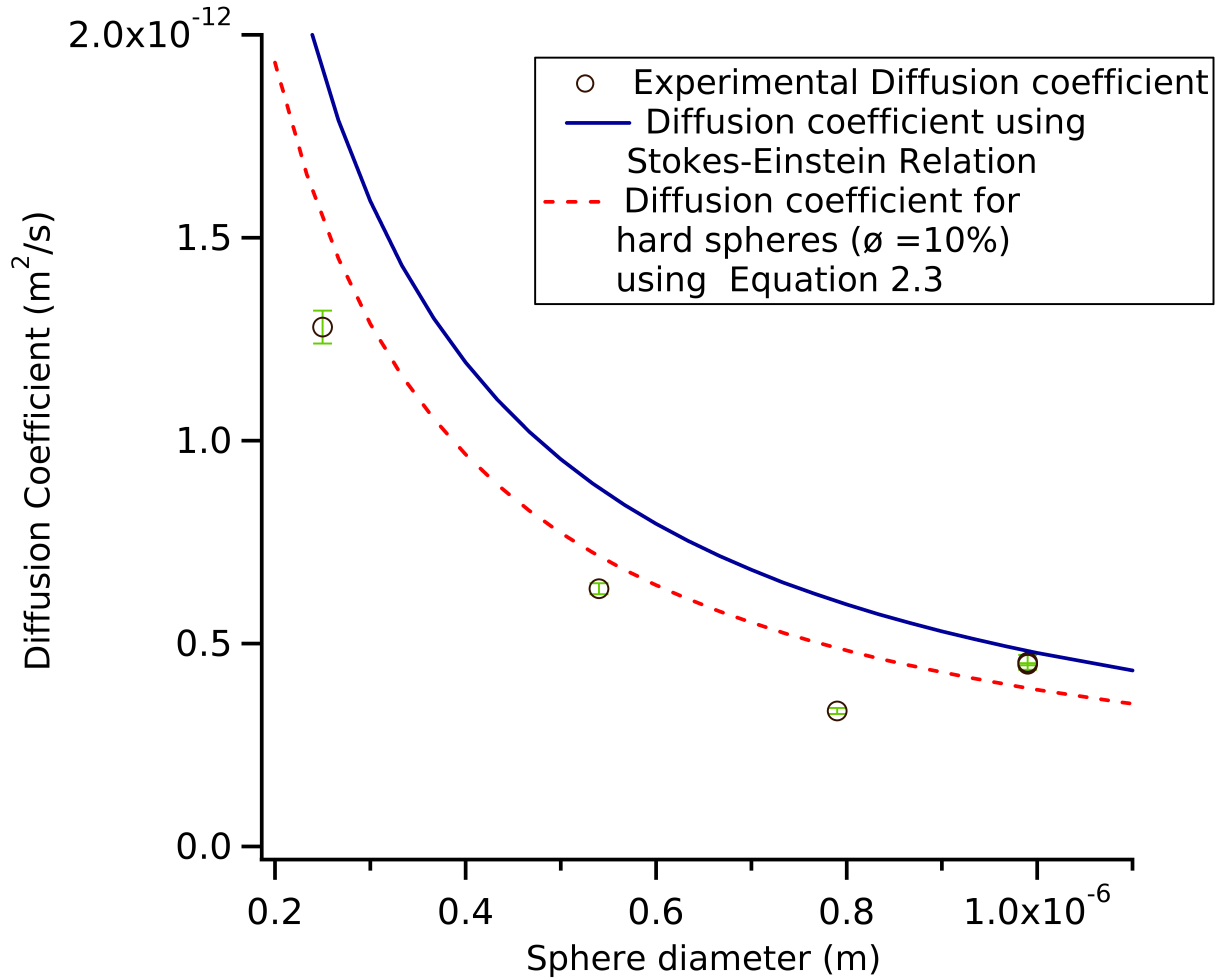
Figure 5.6: Drawn curves showing the Stokes-Einstein prediction (solid curve, Equation 2.2) and a correction for the experimental volume fraction (dashed curve) using Equation 2.3 for $k_s^S = -1.73$ [25].
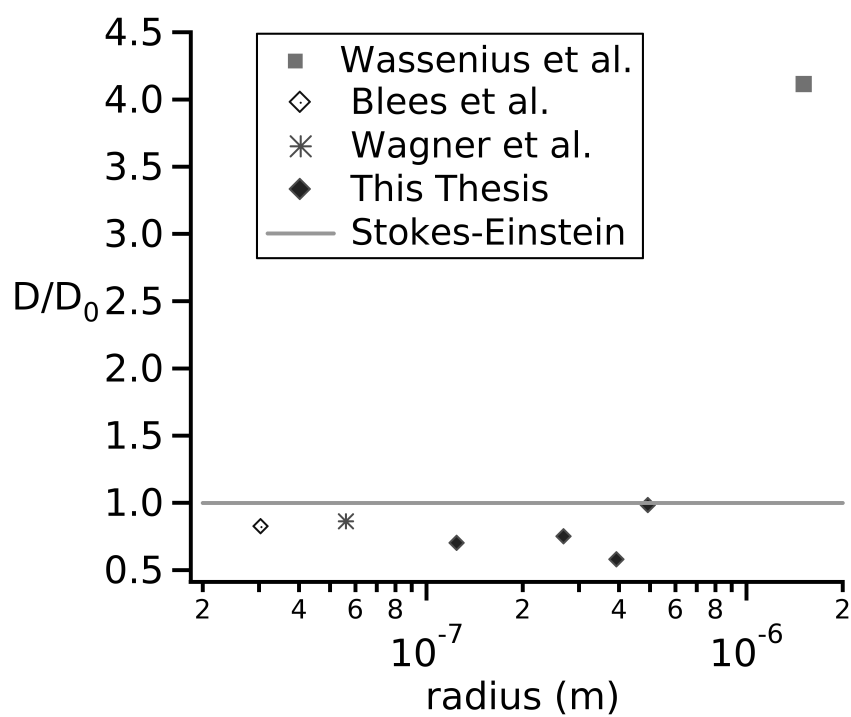
Figure 5.7: Comparison of D/D$_0$ for different PFG NMR experiments. Note that for finite volume fraction, experimental values of D/D$_0$ should be less than unity (solid line).
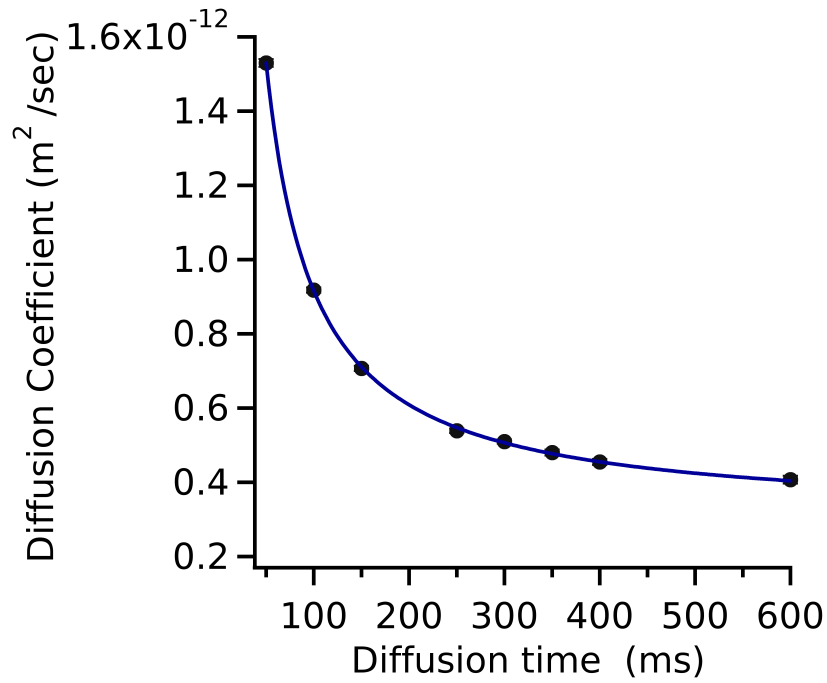
Figure 5.8: Δ dependence of diffusion coefficient for 10% suspension of 0.99 μm polystyrene spheres. Here the diffusion coefficient follows D = A + B/Δ where A=(6.13 ±0.02) × 10^{-11}m^2/s and B=(3.01 ±0.02) × 10^{-13}m^2. We interpret the crossover from sharp Δ dependence to weak Δ dependence as a crossover to true colloid diffusion.

diffusion coefficient represents the diffusion of oil inside the sphere. As the random motion of oil is restricted by the boundary of the sphere, diffusion coefficient of oil varies with Δ. So for $\Delta \geq 300$ ms, we probe the colloidal diffusion. For $\Delta \approx 500$ ms, $\Delta \approx \tau_1$ (the interparticle interaction distance), and the measured colloidal diffusion coefficient is becoming more sensitive to interparticle collisions.

5.3 A Binary Mixture

5.3.1 1D Spectrum

In the binary mixture we had tri-methyl phenyl silane in 0.99 μm particles and p-xylene in 0.79 μm particles. The 1D spectrum is shown in Figure 5.9

5.3.2 Simultaneous Measurement of Two Species

From the binary mixture, we obtained simultaneous signal attenuations for both large and small particles (Figure 5.10) and thus the diffusion coefficients of two species simultaneously. Diffusion coefficients for 0.99 μm and 0.79 μm are $(4.11 \pm 0.1) \times 10^{-13}$ m^2/sec and $(4.79 \pm 0.1) \times 10^{-13}$ m^2/sec respectively (Figure 5.10 and solid spheres in Figure 5.11). Comparison of these data with hydrodynamic theory (Equation 2.8 and Equation 2.9) requires the value of diffusion coefficients at dilute limit (D_0). Using the ideal Stokes-Einstein value rather than an experimentally measured D_0, we find that the diffusion coefficients for the binary mixture are $\approx 7\%$ larger than that predicted by hydrodynamic theory (Equation 2.8 and Equation 2.9). An experimental measurement of diffusion coefficient at infinite dilution can be obtained by measuring the volume fraction dependence of the diffusion coefficient, which is to be done in future. But the ratio of values of diffusion coefficient for two particles in the same binary suspension are close to the particle size ratio, which is expected for dilute suspension.

5.4 Discussion

We obtain spectrally-resolved NMR signals for colloidal microspheres in aqueous suspension. The signal arises not from the colloid itself but from oil absorbed within the porous colloid matrix. PFG-NMR studies exhibit a non-mono-exponential signal attenuation curve (Figure 5.2) indicating that oil undergoes diffusion in a restricted geometry.

Figure 5.9: 1D spectrum of binary mixture of 0.99 μ and 0.79 μ spheres with tri-methyl phenyl silane and p-xylene inside respectively. The peaks are (A) Phenyl peaks from both p-xylene and tri-methyl phenyl silane, (B) Water peak, (C) Methyl peak of p-xylene.(D) Methyl peak of silane. C and D peaks are separated by 2 ppm.
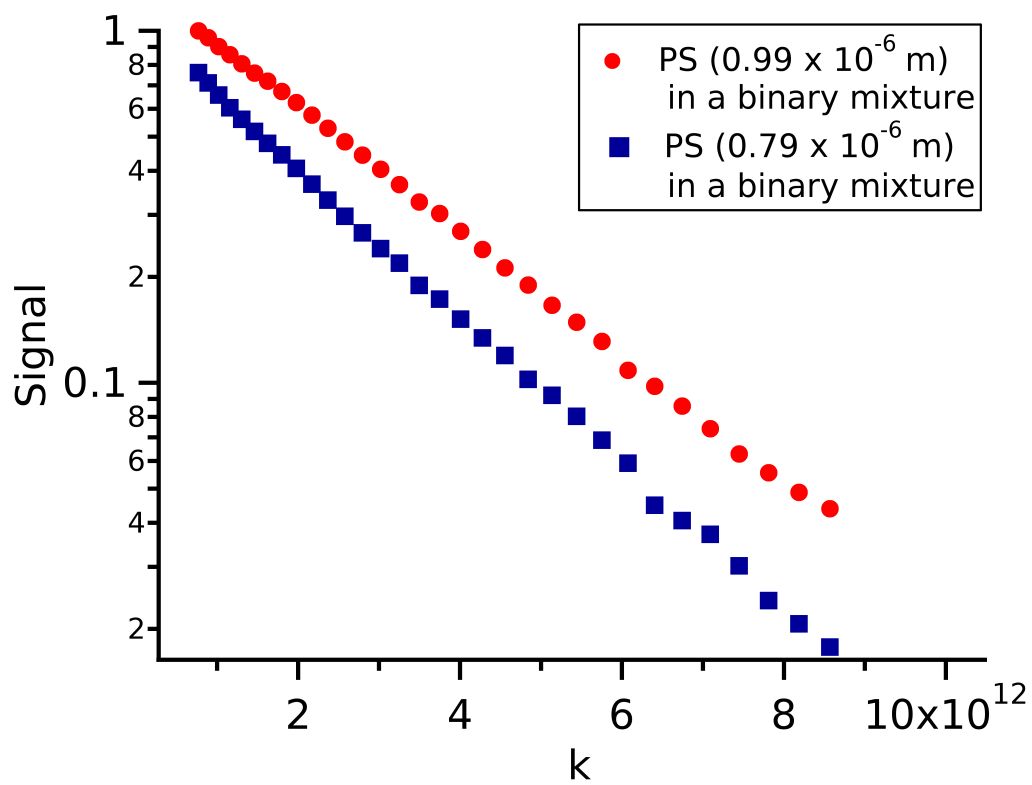
Figure 5.10: Signal attenuation for both large 0.99 μm and small 0.79 μm particles in a binary mixture.
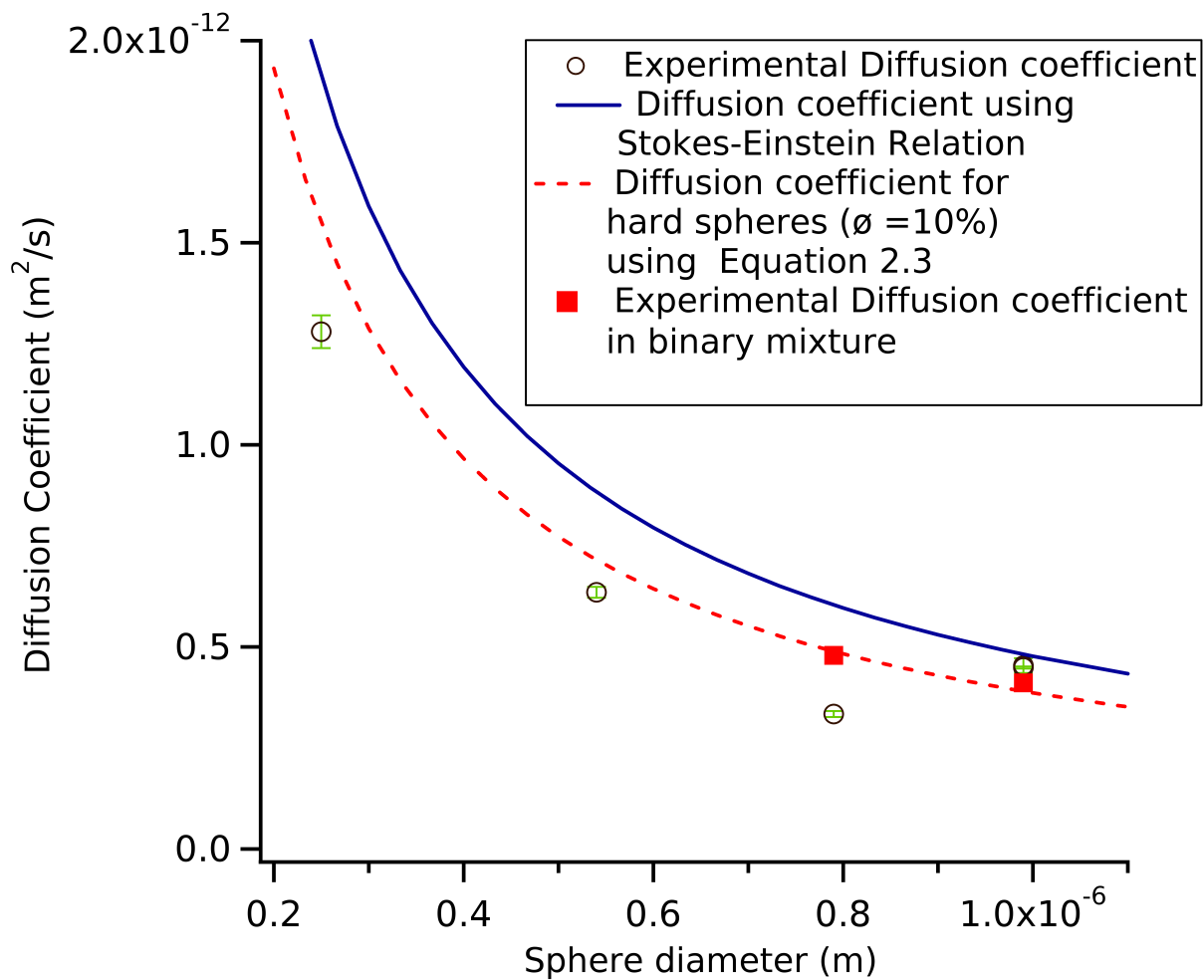
Figure 5.11: Diffusion coefficient of both large and small spheres in binary mixture are shown (filled square). Comparison of these data requires the values of diffusion coefficients at dilute limit (D_0).

We hypothesized a simple form of restricted diffusion for the oil in the colloid. We simply assumed that the oil had an effectively lower different diffusion coefficient in porous polystyrene but still experienced restrictions simply due to the sphere boundary (as in Equation 5.2 to Equation 5.4). Our simple hypothesis for diffusion in a spherical cavity is not upheld by experiments implying that a more complicated theory is needed (simulation of xylene in porous medium that is itself a sphere executing a random walk). However at large gradient strengths, the signal attenuation appears to have an asymptotic mono-exponential form (Figure 5.5). Using this asymptote we get reasonably good agreement with theoretical expectations. In particular, all diffusion coefficients are below the ideal value at infinite dilution, which is an upper bound. Deviations from the hydrodynamic theory must be addressed with systematic experiments as a function of volume fraction. Our PFG-NMR measurements are signal-limited for volume fractions less than 10%. However at low volume volume fractions (1%) confocal microscopy experiments can be carried out to yield diffusion coefficients of infinite dilution. Dependence on Δ implies some form of restricted diffusion. Moreover, the dependence on D at large Δ ($\Delta \approx 500$ ms) suggests that we are probing the slowing down of colloid diffusion due to interparticle interactions.

We are able to probe bidisperse colloidal suspensions successfully using PFG NMR, and simultaneously obtain diffusion coefficients for each species.

Chapter 6

CONCLUSIONS

6.1 Summary

In this thesis we devised a synthesis scheme to make colloidal particles NMR-visible as well as visible by fluorescence laser-scanning confocal microscopy. This was done by making 'oil'-infused colloidal particles, by mixing a water-insoluble organic liquid - either p-xylene or triphenyl methyl silane - with a colloidal suspension of polystyrene microspheres and ultrasonicating until it was absorbed within the microspheres. A dissolved fluorescent dye in the oil made the particles fluorescent. We used the fluorescence to characterize the uniformity of the oil absorption by confocal microscopy. We used measurements of conductivity to ensure that our system was hard-sphere like.

The synthesized suspensions of colloids were probed by PFG-NMR. Since we probe diffusion of colloids via diffusion of the oil absorbed in it, the signal attenuation has multiple effects. First, oil diffuses within the pores of the polystyrene that makes up the colloidal spheres. Second, the boundaries of the spheres act as restrictions for colloid diffusion. Third, the (slower) motion of colloids contributes to the measured oil diffusion. The third effect is most important at high gradient field strengths.

Treating the polymer sphere as a simple spherical cavity, we attempted to fit the entire signal attenuation curve at all gradient strengths. Such a fit is not possible, suggesting a more complicated model for diffusion within the polystyrene matrix. However, by extracting the asymptotic behavior at high gradient field strengths (the maximum value used was 1100 G/cm), we were able to obtain true colloid diffusion coefficients for monodisperse suspensions at different particle sizes. The experimental results are in reasonable agree-

ment with hydrodynamic theory.

The dependence of diffusion coefficient on diffusion time Δ, displayed an expected slowing down at large diffusion times when colloid-colloid interaction becomes more important. It also suggests that both short-time and long-time diffusion coefficients can be accessible in these studies.

We successfully measured diffusion coefficients for two particle species (a 'binary colloidal mixture') simultaneously by PFG-NMR which, as a result, will allow studies of binary colloidal suspensions as a function of colloid sizes and number ratios for different volume fractions.

The model system presented in this thesis establishes that the study of the dynamics at colloidal phase transitions is possible using PFG-NMR.

6.2 Future Work

Our goal is to study the dynamics of hard sphere colloidal suspensions at phase transitions. A systematic study requires that we account for the restricted diffusion of oil (xylene/TPS) quantitatively so the entire signal attenuation curve can be fit. The measurement of diffusion coefficient as a function of Δ, will allow us to extract both the short and long time self-diffusion coefficients in one system (as well as cross-over intermediate values). This would be an important development in the study of colloidal dynamics.

Using PFG-NMR we can measure the diffusion coefficient for a colloidal suspension of volume fraction greater than 10%. Confocal microscopy is, on the other hand, limited to volume fractions less than 3%. As our particles are NMR-visible as well as fluorescent labeled, we will use particle tracking confocal microscopy at low volume fractions to obtain single-species diffusion coefficients to the dilute limit (this is an experimental alternative to using the Stokes-Einstein relation). We also plan to study the volume fraction dependence of diffusion coefficients both for mono-disperse and bi-disperse hard sphere colloidal suspensions. This will allow us to test the validity of hydrodynamic theory for these systems.

In the case of binary suspensions, on increasing volume fraction one should observe (for different size ratios and number ratios) a coupling of diffusion coefficients leading eventually at high packing to glassy behavior. The onset

of glassy behavior as a function of particle size ratios and volume fractions has been probed theoretically but not in detail experimentally. We will approach this regime on increasing particle volume fraction above 55%. The goal is therefore to study binary mixtures for various particle size ratios and number ratios in order to obtain detailed dynamics of concentrated colloidal phases such as in concentrated colloidal fluid FCC and glass phases.

Bibliography

[1] R. M. Pashley and M. E. Karaman. *Applied colloid and surface chemistry*. John Wiley and Sons Ltd, England, 2004.

[2] W. B. Russel, D. A. Saville, and W. R. Schowalter. *Colloidal dispersions*. Cambridge University Press, England, 1989.

[3] D. Frenkel. Soft condensed matter. *Physica A*, 313:1, 2002.

[4] A. Yethiraj. Tunable colloids: control of colloidal phase transitions with tunable interactions. *Soft Matter*, 3:1099, 2007.

[5] A. D. Dinsmore, A. G. Yodh, and D. J. Pine. Phase diagrams of nearly-hard-sphere binary colloids. *Phys. Rev. E*, 52:4045, 1995.

[6] S. Asakura and F. Oosawa. Interaction between particles suspended in solutions of macromolecules. *J. Polymer Science*, 33:183, 1958.

[7] R. J. Hunter. *Foundations of colloid science, Volume I*. Clarendon Press, Oxford, 1987.

[8] D. F. Evans and H. Wennerstrom. *The colloidal domain where physics, chemistry, biology and technology meet*. VCH, New York, 1994.

[9] E. J. W. Verwey and J. Th. G. Overbeek. *Theory of the stability of lyophobic colloids*. Elsevier, New York, 1948.

[10] R. Lee-Desautels. *Theory of van der Waals forces as applied to particulate materials*. Educ. Reso. Part. Techn., 2005.

[11] B. Hakansson, R. Pons, and O. Söderman. Structure determination of a highly concentrated w/o emulsion using pulsed-field-gradient spin-echo nuclear magnetic resonance "diffusion diffractograms". *Langmuir*, 15:988, 1999.

[12] W. J. Briels. *Theory of Polymer Dynamics*. 1998.

[13] K. Höfler. *Simulation and modeling of mono- and bidisperse suspensions.* University of Stuttgart, 2000.

[14] T. G. M. van de Ven. *Colloidal hydrodynamics.* Academic Press Limited, London, 1989.

[15] G. K. Batchelor. Sedimentation in a dilute dispersion of spheres. *J. Fluid Mech.*, 52:245, 1972.

[16] G. K. Batchelor. Sedimentation in a dilute dispersion of spheres. *J. Fluid Mech.*, 52:245, 1972.

[17] R. J. Speedy. The hard sphere glass transition. *Molecular Physics*, 95:169, 1998.

[18] D. H. Everett. Definitions, terminology and symbols in colloid and surface chemistry. *IUPAC*, 1971.

[19] V. Prasad, D. Semwogerere, and E. R. Weeks. Confocal microscopy of colloids. *J. of Phys.: Condensed Matter*, 19:1, 2007.

[20] F. Sciortino and P. Tartaglia. Glassy colloidal systems. *Advances in Physics*, 54:471, 2005.

[21] W. van Megen and P. N. Pusey. Dynamic light-scattering study of the glass transition in a colloidal suspension. *Phys. Rev. A*, 43:5429, 1991.

[22] Z. D. Cheng, P. M. Chaikin, S. Phan, and W. B. Russel. On the nature of the divergence in the low shear viscosity of colloidal hard-sphere dispersions. *Phys. Rev. E.*, 65:041405, 2002.

[23] G. K. Batchelor. Brownian diffusion of particles with hydrodynamic interactions. *J. Fluid Mech.*, 74:1, 1976.

[24] B. U. Felderhof. Diffusion of interacting brownian particles. *J. Phys. Ser. A.*, 11:929, 1978.

[25] M. Muthukumar and K. F. Freed. Cluster expansion for concentration dependence of cooperative friction coefficients for suspensions of interacting spheres. *J. Chem. Phys.*, 78:511, 1983.

[26] B. U. Felderhof. Hydrodynamic interaction between two spheres. *Physica A*, 89:373, 1977.

[27] N. Yoshida. Concentration dependence of the self-diffusion coefficient of hard spheres in solution. *Chem. Phys. Lett.*, 101:555, 1983.

[28] B. Cichocki and B. U. Felderhof. Long-time self-diffusion coefficient and zero-frequency viscosity of dilute suspensions of spherical brownian particles. *J. Chem. Phys.*, 89:3705, 1988.

[29] M. H. Blees, J. M. Geurts, and J. C. Leyte. Self-diffusion of charged polybutadiene latex particles in water measured by pulsed field gradient nmr. *Langmuir*, 12:1947, 1996.

[30] H. Wassenius, M. Nydén, and B. Vincent. Nmr diffusion studies of translational properties of oil inside core-shell latex particles. *J. Coll. Interface Sci.*, 264:538, 2003.

[31] U. Geigenmüeller and P. Mazur. A simple formula for the short-time self-diffusion coefficient in concentrated suspensions. *Physica A*, 146:657, 1987.

[32] M. Medina-Noyola. Long-time self-diffusion in concentrated colloidal dispersions. *Phys. Rev. Lett.*, 60:2705, 1988.

[33] A. van Blaaderen, J. Peetermans, G. Maret, and J. K. G. Dhont. Long-time self-diffusion of spherical colloidal particles measured with fluorescence recovery after photobleaching. *J. Chem. Phys.*, 96:4591, 1992.

[34] S. I. Henderson and W. van Megen. Metastability and crystallization in suspensions of mixtures of hard spheres. *Phys. Rev. Lett.*, 80:877, 1998.

[35] S. Martin, G. Bryant, and W. van Megen. Crystallization kinetics of polydisperse colloidal hard spheres: experimental evidence for local fractionation. *Phys. Rev. E*, 67:061405, 2003.

[36] S. R. Williams, I. K. Snook, and W. van Megen. Molecular dynamics study of the stability of the hard sphere glass. *Phys. Rev. E.*, 64:021506, 2001.

[37] G. K. Batchelor. Diffusion in a dilute polydisperse system of interacting spheres. *J. Fluid Mech.*, 131:155, 1983.

[38] G. K. Batchelor and C. S. Wen. Sedimentation in a dilute polydisperse system of interacting spheres. part 2. numerical results. *J. Fluid Mech.*, 124:495, 1982.

[39] J. N. Roux, J. L. Barrat, and J. P. Hansen. Dynamical diagnostics for the glass transition in soft-sphere alloys. *J. Phys. : Condensed Matter*, 1:7171, 1989.

[40] G. Foffi, W. Götze, F. Sciortino, P. Tartaglia, and Th. Voigtmann. Mixing effects for the structural relaxation in binary hard-sphere liquids. *Phys. Rev. Lett.*, 91:085701, 2003.

[41] W. Götze and Th. Voigtmann. Effect of composition changes on the structural relaxation of a binary mixture. *Phys. Rev. E*, 67:021502, 2003.

[42] S. R. Williams and W. van Megen. Motions in binary mixtures of hard colloidal spheres: melting of the glass. *Phys. Rev. E*, 64:041502, 2001.

[43] A. Imhof and K. G. Dhont. Long-time self-diffusion in binary colloidal hard-sphere dispersions. *Phys. Rev. E*, 52:6344, 1995.

[44] E. R. Weeks, J. C. Crocker, A. C. Levitt, A. Schofield, and D. A. Weitz. Three-dimensional direct imaging of structural relaxation near the colloidal glass transition. *Science*, 287:627, 2000.

[45] A. Imhof and J. K. G. Dhont. Experimental phase diagram of a binary colloidal hard-sphere mixture with a large size ratio. *Phys. Rev. Lett.*, 75:1662, 1995.

[46] P. Bartlett, R. H. Ottewill, and P. N. Pusey. Freezing of binary mixtures of colloidal hard spheres. *J. Chem. Phys*, 93:1299, 1990.

[47] P. N. Pusey. The dynamics of interacting brownian particles. *J. Phys. A*, 8:1433, 1975.

[48] J. C. Brown, P. N. Pusey, J. W. Goodwin, and R. H. Ottewill. Light scattering study of dynamic and time-averaged correlations in dispersions of charged particles. *J. Phys. A*, 8:664, 1975.

[49] R. H. Ottewill. *In colloidal dispersions*. Royal Society of Chemistry, London, 1981.

[50] J. Wagner, W. Härtl, and H. Walderhaug. Long time self-diffusion in suspensions of highly charged colloids: A comparison between pulsed field gradient nmr and brownian dynamics. *J. Chem. Phys.*, 114:975, 2001.

[51] D. A. McQuarrie. *Statistical mechanics*. Harper and Row, New York.

[52] W. van Megen and S. M. Underwood. Dynamic-light-scattering study of glasses of hard colloidal spheres. *Phys. Rev. E*, 47:248, 1993.

[53] A. D. Dinsmore, E. R. Weeks, V. Prasad, A. C. Levitt, and D. A. Weitz. Three-dimensional confocal microscopy of colloids. *Appl. Opt.*, 40:4152, 2001.

[54] J. C. Crocker and D. A. Grier. Methods of digital video microscopy for colloidal studies. *J. Coll. Interface Sci.*, 179:298, 1996.

[55] A. Imhof, A. van Blaaderen, G. Maret, J. Mellema, and J.K.G. Dhont. A comparison between the long-time self-diffusion and low shear viscosity of concentrated dispersions of charged colloidal silica spheres. *J. Chem. Phys.*, 100:2170, 1994.

[56] K. I. Momot and P. W. Kuchel. Pfg nmr diffusion experiments for complex systems. *Concepts in Magnetic Resonance Part A*, 28A:249, 2006.

[57] O. Söderman and P. Stilbs. Nmr studies of complex surfactant systems. *Prog. Nucl. Magn. Resonance Spectrosc.*, 26:445, 1994.

[58] P. T. Callaghan. *Principles of nuclear magnetic resonance.* Oxford Science Publications, London, 1991.

[59] M. H. Levitt. *Spin dynamics.* John Wiley & Sons, Inc., Chichester.

[60] E. L. Hahn. Spin echoes. *Phys.Rev.*, 80:580, 1950.

[61] W. S. Price. *Concepts in magnetic resonance.* John Wiley & Sons, Inc.

[62] H. Y. Carr and E. M. Purcell. Effects of diffusion on free precession in nuclear magnetic resonance experiments. *Phys. Rev.*, 94:630, 1954.

[63] A. Khitrin. *Thermotropic liquid crystals.* Springer.

[64] J. S. Murday and R. M. Cotts. Self-diffusion coefficient of liquid lithium. *J. Chem. Phys.*, 48:4938, 1968.